

# Improving baryon acoustic oscillation measurement with the combination of cosmic voids and galaxies

Cheng Zhao<sup>1,2\*</sup>, Chia-Hsun Chuang<sup>3,4†</sup>, Yu Liang<sup>1</sup>, Francisco-Shu Kitaura<sup>5,6</sup>, Mariana Vargas-Magaña<sup>7</sup>, Charling Tao<sup>8,1</sup>, Marcos Pellejero-Ibanez<sup>5,6</sup>, Gustavo Yepes<sup>9</sup>

<sup>1</sup> *Tsinghua Center for Astrophysics (THCA) & Department of Physics, Tsinghua University, Beijing 100084, P. R. China*

<sup>2</sup> *National Astronomical Observatories, Chinese Academy of Science, Beijing, 100012, P. R. China*

<sup>3</sup> *Kavli Institute for Particle Astrophysics and Cosmology & Physics Department, Stanford University, Stanford, CA 94305, USA*

<sup>4</sup> *Leibniz-Institut für Astrophysik Potsdam (AIP), An der Sternwarte 16, D-14482 Potsdam, Germany*

<sup>5</sup> *Instituto de Astrofísica de Canarias (IAC), C/Vía Láctea, s/n, E-38200, La Laguna, Tenerife, Spain*

<sup>6</sup> *Departamento Astrofísica, Universidad de La Laguna (ULL), E-38206 La Laguna, Tenerife, Spain*

<sup>7</sup> *Instituto de Física, Universidad Nacional Autónoma de México, Apdo. Postal 20-364, México*

<sup>8</sup> *CPPM, Université Aix-Marseille, CNRS/IN2P3, Case 907, 13288 Marseille Cedex 9, France*

<sup>9</sup> *Departamento de Física Teórica and CIAFF, Módulo 8, Facultad de Ciencias, Universidad Autónoma de Madrid, 28049 Madrid, Spain*

2 September 2022

## ABSTRACT

We develop a methodology to optimise the measurement of Baryon Acoustic Oscillation (BAO) from a given galaxy sample. In our previous work, we demonstrated that one can measure BAO from tracers in under-dense regions (voids). In this study, we combine the over-dense and under-dense tracers (galaxies & voids) to obtain better constraints on the BAO scale. To this end, a generalised de-wiggled BAO model with an additional parameter is developed to describe both the BAO peak and the underlying exclusion pattern of void 2PCFs. We show that after applying BAO reconstruction to galaxies, the BAO peak scale of both galaxies and voids are unbiased using the modified model. Furthermore, we exploit a new description of the combined 2PCF for a multi-tracer analysis with galaxies and voids. In simulations, the joint sample improves by more than 10 % the constraint for the post-reconstruction BAO peak position compared to the result from galaxies alone, which is equivalent to an enlargement of the survey volume by 20 %. Applying this method to the BOSS DR12 data, we have an 11 % improvement for the low- $z$  sample ( $0.2 < z < 0.5$ ), but a worse constraint for the high- $z$  sample ( $0.5 < z < 0.75$ ), which is consistent with statistical fluctuations for the current survey volume. We further find that a larger sample gives a more robust improvement due to less statistical fluctuations.

**Key words:** methods: data analysis – statistical – galaxies: statistics – cosmology: observations – large-scale structure of Universe

## 1 INTRODUCTION

The Baryon Acoustic Oscillation (BAO) signature imprinted in the Cosmic Microwave Background (CMB) and in the three dimensional matter distribution at later cosmic times defines a characteristic scale, which is by now commonly used as a standard ruler to determine the expansion of the Universe (Blake & Glazebrook 2003; Seo & Eisenstein 2005). It can be measured as a peak in the 2-point correlation function (2PCF) of different types of matter tracers, such as galaxies (Eisenstein et al. 2005; Cole et al. 2005), quasars

(Ata et al. 2017), the Lyman- $\alpha$  forests (Busca et al. 2013), and potentially the 21 cm line with future experiments (e.g. Chang et al. 2008).

The measurement of BAO peak scale is one of the main scientific goals for a large number of large-scale galaxy surveys, such as SDSS-III/BOSS<sup>1</sup> (Baryon Oscillation Spectroscopic Survey, Eisenstein et al. 2011; Dawson et al. 2013), SDSS-IV/eBOSS<sup>2</sup> (the extended BOSS, Dawson et al. 2016), DESI<sup>3</sup> (Dark Energy Spectroscopic Instrument, Levi et al.

\* E-mail: c-zhao15@mails.tsinghua.edu.cn

† E-mail: chuangch@stanford.edu

<sup>1</sup> <https://sdss3.org/surveys/boss.php>

<sup>2</sup> <http://www.sdss.org/surveys/eboss/>

<sup>3</sup> <http://desi.lbl.gov>

2013), DES<sup>4</sup> (Dark Energy Survey, [Dark Energy Survey Collaboration et al. 2016](#)), LSST<sup>5</sup> (Large Synoptic Survey Telescope, [LSST Dark Energy Science Collaboration 2012](#)), J-PAS<sup>6</sup> (Javalambre Physics of the Accelerating Universe Astrophysical Survey, [Benitez et al. 2014](#)), 4MOST<sup>7</sup> (4-metre Multi-Object Spectroscopic Telescope, [de Jong et al. 2012](#)), Euclid<sup>8</sup> ([Laureijs et al. 2011](#)), and WFIRST<sup>9</sup> (Wide Field Infrared Survey Telescope, [Spergel et al. 2013](#)).

To extract the maximum cosmological information from BAO measurements, many systematical uncertainties have to be taken into account, such as survey geometry, bias, redshift space distortions and gravitational evolution. These aspects have been addressed in the last few years to improve the BAO measurements from galaxy surveys (cf. [Ross et al. 2017](#), and references therein). In particular, ways to linearise the galaxy distribution with so-called BAO reconstruction techniques, enhancing the BAO peak, have been developed and successfully applied ([Weinberg 1992](#); [Eisenstein et al. 2007](#); [Padmanabhan et al. 2012](#); [Noh et al. 2009](#)). This procedure has been interpreted as a way to transfer information encoded in the three and four point statistics to the two point correlation function (cf. [Schmittfull et al. 2015](#)).

It is important to stress that no matter how much a galaxy distribution is linearised by redistributing the position of individual galaxies according to the inferred displacement field, they will trace only the peaks of the density field, leaving a large fraction of the cosmic web under-represented, according to the galaxy bias picture introduced by [Kaiser \(1984\)](#), which is particularly confirmed for Luminous Red Galaxies (LRGs) (cf. e.g. [Kitaura et al. 2015, 2016c](#)). Thus, the linearised galaxy distribution after BAO reconstruction represents at best a truncated Gaussian density field.

The three dimensional distribution of galaxies however, encodes also the information of the troughs within cosmic voids of the density field. In particular, it is possible to guess the depth of such cosmic voids based on the distribution of peaks in the density field, and thus estimate the density field in regions, where there are no data. One could use some Bayesian reconstruction techniques to achieve this (cf. e.g. [Zaroubi et al. 1995](#)). The problem of such approaches is the dependence on the cosmology set in the assumed correlation function, which we want to avoid here (although there are some attempts to do this by sampling the power spectrum, cf. [Kitaura & Enßlin \(2008\)](#)). An alternative is to use pure geometrical arguments to find large regions devoid of galaxies (e.g. [El-Ad & Piran 1997](#); [Way et al. 2015](#); [Zhao et al. 2016](#)). The latter approach yields additional cosmic void tracers (cf. [Liang et al. 2016](#); [Zhao et al. 2016](#)). The combination of this new set of cosmic void tracers with the galaxy distribution permits us to perform a multi-tracer analysis, which has been shown to yield much tighter cosmological constraints (e.g. [Gil-Marín et al. 2010](#); [Bernstein & Cai 2011](#); [Hamaus et al. 2011, 2012](#); [Abramo & Leonard 2013](#); [Ferraro et al. 2015](#)).

Even though the exact void definition is subtle (cf. e.g. [Colberg et al. 2008](#); [Zhao et al. 2016](#), and references therein), it is widely accepted that large voids, or the so called voids-in-voids ([Sheth & van de Weygaert 2004](#)), are tracing troughs of the cosmic density field (for a review, cf. [van de Weygaert & Platen 2011](#)), and have negative bias (e.g. [Hamaus et al. 2014](#); [Zhao et al. 2016](#)). Recently, it has been shown that cosmic voids can be used to measure the BAO signature (cf. [Kitaura et al. 2016a](#); [Liang et al. 2016](#)), although a growth rate estimation is not trivial ([Chuang et al. 2017](#)). We aim at investigating here, how cosmic voids can be combined with the galaxy distribution to improve the estimation of cosmological parameter estimation after applying BAO reconstruction.

In section 2, we begin with a description of the observed and simulated data we used. Then, we present our method of constructing void catalogues and computing 2PCFs as well as the covariances in section 3. Later, in section 4, we develop a modified BAO fitting method. Finally, we measure the BAO peak scale by combining galaxies and voids and discuss the contribution of voids in section 5, and conclude in section 6.

## 2 DATA

In this work we will rely on both observed and simulated data as described below.

### 2.1 Observed Galaxy sample

Our study focus on the distribution of Luminous Red Galaxies (LRGs), as obtained by the Sloan Digital Sky Survey (SDSS) 2.5-meter telescope at Apache Point Observatory, and presented in the final BOSS data release. The spectra are measured using the double-armed BOSS spectrograph, and then classified to measure the redshift ([Bolton et al. 2012](#)), followed by a target selection scheme to generate the final large-scale structure catalogues ([Reid et al. 2016](#)).

The final LRG catalogue consists of over 1.3 million LRGs from both north and south galactic caps, spanning across nearly 10,000 deg<sup>2</sup> on the sky ([Alam et al. 2017](#)). We apply weights to correct for systematical effects, such as fibre collisions and the correlations between target density and both stellar density and seeing ([Reid et al. 2016](#); [Ross et al. 2017](#)), together with the redshift-dependent FKP weight for sample combination ([Feldman et al. 1994](#)).

As in [Alam et al. \(2017\)](#), we further divide the BOSS DR12 LRG sample into two independent redshift bins with nearly equal effective volume,  $0.2 < z < 0.5$  and  $0.5 < z < 0.75$ , denoted hereafter “low- $z$ ” and “high- $z$ ” bins respectively. The corresponding effective redshift for these two bins are 0.38 and 0.61.

### 2.2 Simulated PATCHY halo mocks

To validate our BAO fitting method, we rely on 100 realisations of cubic mock halo catalogues constructed by the Perturbation Theory Catalogue generator of Halo and galaxy distributions (the PATCHY-code, [Kitaura et al. 2014](#)), which uses the Augmented Lagrangian Perturbation Theory (ALPT, [Kitaura & Heß 2013](#)) to generate the dark matter

<sup>4</sup> <http://www.darkenergysurvey.org>

<sup>5</sup> <http://www.lsst.org/lsst/>

<sup>6</sup> <http://j-pas.org>

<sup>7</sup> <https://www.4most.eu>

<sup>8</sup> <http://www.euclid-ec.org>

<sup>9</sup> <http://wfirst.gsfc.nasa.gov>

**Table 1.** Cosmological parameters for the Planck BigMultiDark simulation and PATCHY mocks, with a flat  $\Lambda$ CDM framework.

Parameter	Value
$\Omega_m$	0.307115
$\Omega_b$	0.048206
$\sigma_8$	0.8288
$n_s$	0.96
$h$	0.6777

density field, and then populate haloes with an explicit Eulerian nonlinear and stochastic bias description.

In particular, the side length of the mock box is  $2.5 h^{-1} \text{Gpc}$ , with 960 grids on each side (i.e.,  $960^3$  dark matter particles in total). The PATCHY mock halo catalogues are then generated using the public input parameters (Kita<sup>ura</sup> et al. 2015) that have been calibrated with the Spherical Overdensity (SO) halo catalogue, with the halo number density of  $3.5 \times 10^{-4} h^3 \text{Mpc}^{-3}$ , from the BigMultiDark (BIGMD) Planck  $N$ -body simulations (Klypin et al. 2014) at redshift  $z = 0.56$ , with the cosmological parameters given in Table 1. The number density of haloes is chosen to reproduce the population of LRGs of the BOSS survey, that have the same typical density (e.g. Alam et al. 2017).

It has been shown that both two and three-point statistics of the BIGMD halo catalogue are accurately reproduced by the PATCHY mock haloes (Chuang et al. 2015). We then generate 100 realisations of PATCHY mock halo catalogues using the same input parameters, but varying the random seed for the initial conditions, to estimate the effects of cosmic variance in our analysis.

Furthermore, we have generated the other set of 100 PATCHY realisations, with the same initial conditions and parameters as the realisations above, but replacing the input linear power spectrum with a smoothed power spectrum without BAO wiggles. We call this set of mocks PATCHY non-wiggle mocks. Therefore, the only difference between the non-wiggle mocks and the original PATCHY mocks is the BAO signal.

### 2.3 Simulated MultiDark-PATCHY galaxy catalogues

In addition, to make a robust analysis of uncertainties for the observed data, we use a large number of accurate mock galaxy catalogues. The MultiDark-PATCHY (MD-PATCHY) mock galaxy catalogues are constructed based on the mock halo catalogues generated the same way as in §2.2, but with 10 redshift snapshots (Kita<sup>ura</sup> et al. 2016b). The HADRON code (Zhao et al. 2015) is then applied to assign mass to haloes, followed by the Halo Abundance Matching (HAM, e.g. Nuza et al. 2013) scheme to populate galaxies. Finally, the light-cone mocks are built using the SUGAR code (Rodríguez-Torres et al. 2016), with observational effects such as stellar mass incompleteness and fibre collisions being taken into account.

The MD-PATCHY mocks have been calibrated with BOSS DR12 data, and shown accurate clustering statistics. In this work, we use 1000 realisations of MD-PATCHY mocks. Furthermore, we divide the galaxy mocks into the same two redshift bins as the case of observed data.

## 3 METHOD

In this section we present the methodology to obtain the 2PCF and its covariance for galaxies and cosmic voids after BAO reconstruction.

### 3.1 BAO reconstruction

The BAO reconstruction technique was introduced by Weinberg (1992) and extended by Eisenstein et al. (2007); Noh et al. (2009); Padmanabhan et al. (2009). Since then, it has been widely applied to galaxy catalogues and shown improvements on the precision of BAO peak position measurements in most cases (e.g. Anderson et al. 2012; Padmanabhan et al. 2012; Anderson et al. 2014; Burden et al. 2014; Kazin et al. 2014; Vargas-Magaña et al. 2015; Alam et al. 2017). Therefore, it has become an essential tool for BAO analyses.

The basic idea of BAO reconstruction is to reverse partially the bulk flow of galaxies. In practice, we smooth the galaxy density field using a Gaussian kernel with a smoothing scale  $R$ , and then solve the Lagrangian displacement field of galaxies through the Zel’dovich approximation (Zel’dovich 1970; Croft & Gaztanaga 1997). With the displacement field we are able to move back the galaxies, as well as correct redshift space distortions, thus partially removing the nonlinear effects of structure growth.

Apart from the “standard” BAO reconstruction scheme, a number of alternative or improved methods have been proposed, such as BAO reconstruction with the “infinity compressible” fluid (Mohayaee & Sobolevskii 2008), optimal filters (Tassev & Zaldarriaga 2012), effects of local environments (Achitouv & Blake 2015; Neyrinck et al. 2016), isobaric algorithm (Wang et al. 2017), and iterative algorithm with different smoothing lengths (Schmittfull et al. 2017). Furthermore, some Bayesian methods have been developed to recover accurately the initial density field given a distribution of galaxies (Kita<sup>ura</sup> 2013; Jasche & Wandelt 2013; Wang et al. 2013).

In this work we exploit the standard BAO reconstruction method. In particular, for the PATCHY cubic halo mocks, we use a smoothing scale of  $R = 5 h^{-1} \text{Mpc}$  for BAO reconstruction. While the reconstructed MD-PATCHY DR12 galaxy mocks are the same as those used in Alam et al. (2017), with  $R = 15 h^{-1} \text{Mpc}$ . It has been shown that the difference on smoothing scale does not significantly affect the monopole BAO peak position constraint (Vargas-Magaña et al. 2015). Our studies in this work includes both pre-reconstruction and post-reconstruction cases for all the data and mocks.

### 3.2 Void finding

We apply the DIVE void finding algorithm (Zhao et al. 2016) to the halo or galaxy catalogues to obtain our void samples. It uses the Delaunay Triangulation (DT, Delaunay 1934) technique to partition the space containing a point set into tetrahedra, with the vertices being the points. At the same time, the DT scheme ensures that the circumsphere of the tetrahedra do not have any points inside. We dub these empty spheres DT voids, and use the centres of the spheres for clustering analyses.

For the cubic mocks, we copy the haloes that are closer than  $100 h^{-1}\text{Mpc}$  to the nearest boundary to the opposite outside of the box, and then remove voids found outside the original box, to ensure the periodic boundary condition. The duplicate length is chosen to be larger than the radius of the largest void ( $\sim 40 h^{-1}\text{Mpc}$ ). For light-cone mocks, we simply mask out the voids centred in unobserved regions.

It is worth noting that the complexity of the DIVE algorithm scales as  $\mathcal{O}(n \log n)$ , where  $n$  denotes the number of matter tracers (haloes or galaxies). The high efficiency makes our void finding scheme applicable to clustering statistics with thousands of mock realisations for the state of art survey size.

Furthermore, DIVE requires only a halo or galaxy catalogue in comoving space, without any additional assumptions. The only free parameter for our void definition is a radius cut. It has been shown that the bias and BAO significance vary for different void radius bins, and only large voids are mostly located in expanding regions, with anti-correlations to galaxies or haloes (Liang et al. 2016; Zhao et al. 2016).

We define the optimal radius cut for void selection using the set of mocks for estimating the covariance matrices for observations, by maximising the signal-to-noise ratio of the BAO peak significance, which is expressed by the difference of the amplitude between the BAO peak and the dips on scales smaller and larger than the peak. In particular, for BOSS DR12 like data, Liang et al. (2016) used the MD-PATCHY DR12 galaxy mocks and found an optimal radius cut of  $R_{\text{th}} = 16 h^{-1}\text{Mpc}$ , i.e., we use only voids with radii larger than  $R_{\text{th}}$ . A slice of the distribution of galaxies and voids from BOSS DR12 data is shown in Figure 1.

Since voids are indirect observables, and are defined by haloes or galaxies, we cannot directly apply BAO reconstruction to voids. Instead, we run BAO reconstruction for haloes or galaxies first, followed by DIVE to construct the post-reconstruction void sample. For the light-cone mocks, we use still the original survey masks to remove voids outside the observed area.

In this work, we consider neither systematical weights nor FKP weights for voids. Nevertheless, the 2PCFs of voids do not show significant systematical bias (Kitaura et al. 2016a; Liang et al. 2016). We leave the detailed weighting scheme for voids to a future work.

### 3.3 Correlation function estimator

We compute the monopole 2-point correlation function (2PCF)  $\xi(s)$  for the pre-reconstruction samples using the Landy-Szalay estimator (Landy & Szalay 1993):

$$\xi_{\text{pre}}(s) = \frac{DD(s) - 2DR(s) + RR(s)}{RR(s)}, \quad (1)$$

where  $DD(s)$ ,  $DR(s)$ , and  $RR(s)$  are the number of galaxy pairs with the separation of  $s$  from data-data, data-random, and random-random pairs, normalised by the corresponding number of total pairs respectively. We use a trivial uniformly distributed random catalogue for the cubic mocks, which contains the same number of tracers as the data, and random catalogues generated using the ‘‘shuffled’’ method (Ross et al. 2012; Liang et al. 2016) for light-cone mocks.

For the post-reconstruction case, besides reversing the

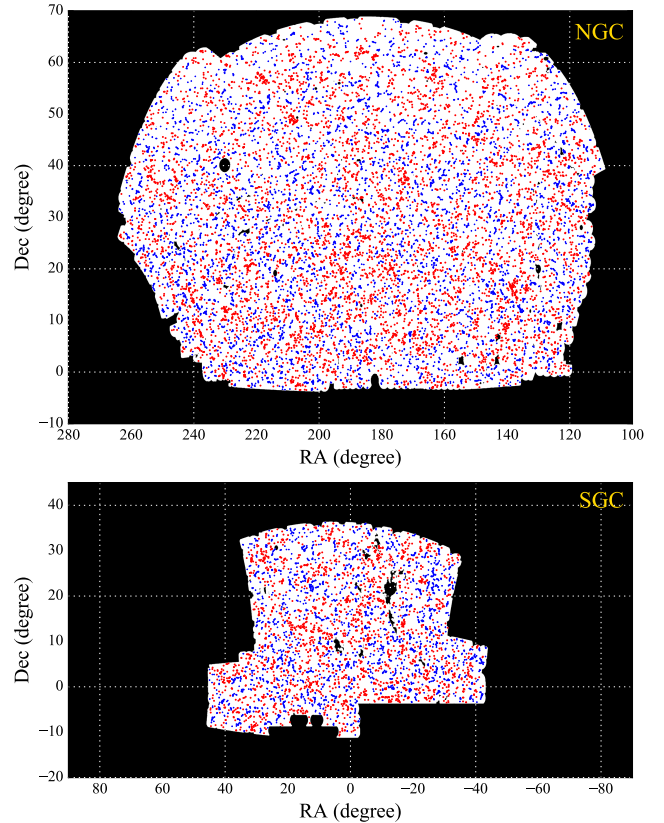


**Figure 1.** Angular distribution of BOSS DR12 LRGs (red points) and the corresponding DT voids with radii  $\geq 16 h^{-1}\text{Mpc}$  (blue points) in the Northern Galactic Cap (NGC, upper panel) and Southern Galactic Cap (SGC, lower panel), within a redshift slice of  $0.498 < z < 0.5$ .

displacement of haloes or galaxies, we also shift the random catalogue by the same displacement field. Denoting the shifted random catalogue by  $S$ , the Landy-Szalay estimator becomes (Padmanabhan et al. 2012)

$$\xi_{\text{post}}(s) = \frac{DD(s) - 2DS(s) + SS(s)}{RR(s)}, \quad (2)$$

where  $D$  is the shifted data catalogue, and  $R$  is the same random catalogue as the pre-reconstruction case.

Since voids are reconstructed by applying the void finder to post-reconstruction halo/galaxy catalogues, there is no displacement field for shifting the randoms. Therefore, we have to use Eq. 1 for estimating the post-reconstruction correlation functions for voids, which does not require the  $S$  catalogue. We construct  $R$  catalogues for pre- and post-reconstruction catalogues separately using the shuffled method described in Liang et al. (2016).

Throughout this paper, the range of separation for the 2PCFs is always  $s \in [0, 200] h^{-1}\text{Mpc}$ , with the bin size of  $5 h^{-1}\text{Mpc}$ . Furthermore, the random catalogues for cubic mocks contains the same number of tracers as the data, and the number of (shifted) random tracers for the light-cone mocks are always 20 times than that of the corresponding data for both galaxies and voids.

### 3.4 Covariance matrices

We estimate the covariance matrices of the 2PCFs by using the sample covariance of mocks:

$$\mathbf{C}_{s,ij} = \frac{1}{N_m - 1} \sum_{k=1}^{N_m} [\xi_k(s_i) - \bar{\xi}(s_i)][\xi_k(s_j) - \bar{\xi}(s_j)], \quad (3)$$

where  $N_m$  is the number of mocks,  $\xi_k(s)$  is the 2PCF of the  $k$ -th mock, and  $\bar{\xi}(r)$  is the mean 2PCF of all the mocks.

Then, to evaluate the  $\chi^2$  for the fitting, we estimate the unbiased inverse covariance matrix by (Hartlap et al. 2007; Percival et al. 2014)

$$\mathbf{C}^{-1} = \mathbf{C}_s^{-1} \frac{N_m - N_{\text{bins}} - 2}{N_m - 1}, \quad (4)$$

where  $N_{\text{bins}}$  is the number of data bins used for the fitting.

## 4 BAO FITTING

The typical de-wiggled model for galaxies (Xu et al. 2012) does not work well for voids (cf. §4.3), mainly due to the oscillation patterns induced by void exclusion effects (e.g. Zhao et al. 2016). Therefore, we present in this section an improved BAO model, and discuss some details for the fitting.

### 4.1 The typical de-wiggled model

We follow Xu et al. (2012) for computing the template 2PCF:

$$\xi_t(s) = \int \frac{k^2 dk}{2\pi^2} P_t(k) j_0(ks) e^{-k^2 a^2}, \quad (5)$$

where  $P_t(k)$  is the template power spectrum,  $j_0$  is the 0-order spherical Bessel function of the first kind (the sinc function), and  $a$  is a factor for the Gaussian high- $k$  damping. We use  $a = 1 h^{-1} \text{Mpc}$ , as in Xu et al. (2012).

The template power spectrum is generated by

$$P_t(k) = [P_{\text{lin}}(k) - P_{\text{lin,nw}}(k)] e^{-k^2 \Sigma_{\text{nl}}^2 / 2} + P_{\text{lin,nw}}(k). \quad (6)$$

Here,  $P_{\text{lin}}(k)$  is the linear power spectrum,  $P_{\text{lin,nw}}(k)$  is the non-wiggle (free of BAO wiggles) power spectrum, and  $\Sigma_{\text{nl}}$  is the damping parameter for BAO. For the cubic halo mocks, we use the input power spectra when generating the mocks for the fitting, hence the fiducial cosmology is exactly the ‘‘true’’ cosmology. While for the light-cone mocks and BOSS DR12 data,  $P_{\text{lin}}(k)$  is obtained by the CAMB<sup>10</sup> (Lewis et al. 2000) software, and  $P_{\text{lin,nw}}(k)$  is computed using the fitting formulae of Eisenstein & Hu (1998), with the fiducial cosmological parameters given by Table 2.

Then, we fit the 2PCFs using the forms in Xu et al. (2012):

$$\xi_{\text{model}}(s) = B^2 \xi_t(\alpha s) + A(s), \quad (7)$$

where

$$A(s) = \frac{a_1}{s^2} + \frac{a_2}{s} + a_3. \quad (8)$$

Here,  $B$  is the normalisation parameter (it absorbs the bias

**Table 2.** The fiducial cosmological parameters for the comoving space sample construction and BAO fitting, with a flat  $\Lambda$ CDM framework.

Parameter	Value
$\Omega_m$	0.31
$\Omega_b$	0.048143
$\sigma_8$	0.8
$n_s$	0.97
$h$	0.676

factor  $b$ ),  $\alpha$  is the scale dilation parameter, and  $a_1$ ,  $a_2$ , and  $a_3$  are the linear nuisance parameters.

Indeed,  $\alpha$  is the measurement of the baryon acoustic scale (the BAO peak position) relative to the fiducial cosmology, which can be expressed as

$$\alpha = \alpha_{\perp}^{2/3} \alpha_{\parallel}^{1/3}, \quad (9)$$

where  $\alpha_{\perp}$  and  $\alpha_{\parallel}$  are the dilation in the transverse and line-of-sight directions respectively:

$$\alpha_{\perp} = \frac{D_A(z) r_d^{\text{fid}}}{D_A^{\text{fid}}(z) r_d} \quad (10a)$$

$$\alpha_{\parallel} = \frac{H^{\text{fid}}(z) r_d^{\text{fid}}}{H(z) r_d}. \quad (10b)$$

Here,  $D_A(z)$  and  $H(z)$  are the angular diameter distance and Hubble parameter respectively, and  $r_d$  is the sound horizon at radiation drag.

In summary, we have 6 free parameters in this model, they are  $\Sigma_{\text{nl}}$ ,  $B$ ,  $a_1$ ,  $a_2$ ,  $a_3$ , and  $\alpha$ .

### 4.2 Parameter inference

Since  $\alpha$  represents the BAO peak position, and is what we want for measuring the geometry of the Universe, we are particularly interested in the fitting results on  $\alpha$ , including the best-fit value and error. To this end, we sample  $\alpha$  on uniform grids in the range [0.8, 1.2], with a bin size of 0.002, and compute the  $\chi^2(\alpha)$  with

$$\chi^2(\alpha) = (\boldsymbol{\xi}_d - \boldsymbol{\xi}_{\text{model}})^T \mathbf{C}^{-1} (\boldsymbol{\xi}_d - \boldsymbol{\xi}_{\text{model}}), \quad (11)$$

where  $\boldsymbol{\xi}_d$  is the measured 2PCF, and  $\boldsymbol{\xi}_{\text{model}}$  is the model.

We then minimise  $\chi^2(\alpha)$  for each value of  $\alpha$ . In particular, for the nuisance parameters  $a_1$ ,  $a_2$ , and  $a_3$ , we use the linear least-square estimator. And we rely on the Powell’s function minimising method (e.g. Press et al. 2007) for  $\Sigma_{\text{nl}}$  and  $B$ .

Assuming a Gaussian-like likelihood of  $\alpha$ , the probability distribution function of  $\alpha$  is

$$L(\alpha) \propto \exp(-\chi^2(\alpha)/2), \quad (12)$$

where the normalisation factor is chosen to fulfil

$$\int_{0.8}^{1.2} L(\alpha) d\alpha = 1. \quad (13)$$

Then, the variance of  $\alpha$  is

$$\sigma^2(\alpha) = \int_{0.8}^{1.2} (\alpha - \mu(\alpha))^2 L(\alpha) d\alpha, \quad (14)$$

where the expectation value of  $\alpha$  is given by

$$\mu(\alpha) = \int_{0.8}^{1.2} \alpha L(\alpha) d\alpha. \quad (15)$$

<sup>10</sup> <http://camb.info>

**Table 3.** Fitting results of the de-wiggled model for the mean 2PCF of 100 pre-reconstruction PATCHY cubic mocks.

Parameter	Halo	Void
$\bar{\alpha} - 1$	0.00394	0.00534
$\sigma_\alpha$	0.00389	0.00528
$\Sigma_{\text{nl}}$	6.595	0
$B$	1.555	1.169
$\chi^2_{\text{min}}$	0.198	14.9

We have ensured that the probability distribution  $L(\alpha)$  outside the range  $\alpha \in [0.8, 1.2]$  is negligible, and the bin size 0.002 is fine enough, i.e., enlarging the fitting range or reducing the bin size of  $\alpha$  does not change the fitting results. Furthermore, we have checked fitting all the 6 parameters together using the MULTINEST<sup>11</sup> (Feroz & Hobson 2008; Feroz et al. 2009, 2013) tool, and got consistent results with the method mentioned above.

### 4.3 Fitting results with the typical de-wiggled model

To verify our BAO fitting method, we apply the fitting procedure to the 2PCFs of both pre-reconstruction haloes and voids from the PATCHY mocks in cubic volume. The comparison of 2PCFs of haloes and voids are shown in Figure 2. In particular, to reduce the impact of cosmic variance, we fit the model to the mean 2PCF of 100 realisations of mocks, with the covariance matrix drawn from the same suites of mocks.

Furthermore, using the wiggle free realisations of PATCHY mocks, we split the 2PCFs as well as the best-fit model curves into BAO (wiggle) and continuous (non-wiggle) components, and then decompose the model to fit the two parts respectively.

The results for haloes and voids are shown in Figure 3 and Figure 4 respectively. One can see that the typical de-wiggled model works well for haloes, but the wiggled component of the model is sub-optimal for voids. We further list explicitly the fitted parameters in Table 3. The large minimum  $\chi^2$  value also suggests that the BAO model can be improved.

### 4.4 The modified de-wiggled model

Since the bottom panel of Figure 4 shows that the continuous component of the measured 2PCF can be well fitted for voids, we then focus on improving the wiggled component of the model, which comes from the first term on the right hand side of Eq. 6:

$$P_t^{\text{w}}(k) = [P_{\text{lin}}(k) - P_{\text{lin,nw}}(k)]e^{-k^2\Sigma_{\text{nl}}^2/2}. \quad (16)$$

Note that the BAO signal here is modelled by the linear and wiggle-free matter power spectra, we use the damping factor  $e^{-k^2\Sigma_{\text{nl}}^2/2}$  and a bias factor  $B$  (Eq. 7) to approximate the halo BAO feature. However, this approximation is not guaranteed to be valid for voids as well. To verify this, using

the non-wiggle PATCHY mocks, we plot the difference between the power spectrum and the corresponding non-wiggle one for both galaxies and voids, i.e.

$$P_{\text{diff}}^{\text{halo,w}}(k) = P^{\text{halo}}(k) - P_{\text{nw}}^{\text{halo}}(k), \quad (17a)$$

$$P_{\text{diff}}^{\text{void,w}}(k) = P^{\text{void}}(k) - P_{\text{nw}}^{\text{void}}(k), \quad (17b)$$

and then compare them with that of dark matter in the linear regime in Figure 5. One can see that the damping factor (a descending exponential function) works only for haloes, but fails for voids. Therefore, the BAO model for voids need to be modified.

We then use the ratio of the power spectrum and the corresponding non-wiggle one to indicate the BAO signal, i.e.

$$P^{\text{w}'}(k) = \frac{P(k)}{P_{\text{nw}}(k)} - 1, \quad (18)$$

and plot the results in Figure 6. It shows that for both haloes and voids, the wiggled components expressed in this way can be estimated by the linear one with a damping factor. Accordingly, we construct a model that is similar but different to that in Eq. 6:

$$\frac{P_t(k)}{P_{t,\text{nw}}(k)} - 1 = \left( \frac{P_{\text{lin}}(k)}{P_{\text{lin,nw}}(k)} - 1 \right) e^{-k^2\Sigma_{\text{nl}}^2/2}, \quad (19)$$

namely

$$P_t(k) = \left[ (P_{\text{lin}}(k) - P_{\text{lin,nw}}(k))e^{-k^2\Sigma_{\text{nl}}^2/2} + P_{\text{lin,nw}}(k) \right] \cdot \frac{P_{t,\text{nw}}(k)}{P_{\text{lin,nw}}(k)}. \quad (20)$$

Note that compared to Eq. 6, this new power spectra model contains only an extra factor  $P_{t,\text{nw}}(k)/P_{\text{lin,nw}}(k)$ .

To parameterise this extra term in the new BAO model, we plot the measured  $P_{\text{tracer,nw}}(k)/P_{\text{lin,nw}}(k)$  for both haloes and voids from the PATCHY cubic mocks in Figure 7. It shows that the term for haloes is nearly a constant, which explains why the model in Eq. 6 works well for haloes. But for voids, the curve is far away from flat. We then use a simple parabola to model this term (features on large  $ks$  are greatly suppressed by the damping factor):

$$\frac{P_{t,\text{nw}}(k)}{P_{\text{lin,nw}}(k)} = c_0 + c_2k^2. \quad (21)$$

Considering that a constant factor can be absorbed by the parameter  $B$  in Eq. 7, we can rewrite Eq. 20 as

$$P_t(k) = \left[ (P_{\text{lin}}(k) - P_{\text{lin,nw}}(k))e^{-k^2\Sigma_{\text{nl}}^2/2} + P_{\text{lin,nw}}(k) \right] \cdot (1 + ck^2). \quad (22)$$

Moreover, since the linear non-wiggle matter power spectrum  $P_{\text{lin,nw}}(k)$  is a smooth function, the factor  $(1 + ck^2)$  is coupled with the nuisance polynomial parameters. We can further simplify the BAO model as

$$P_t(k) = (P_{\text{lin}}(k) - P_{\text{lin,nw}}(k))(1 + ck^2)e^{-k^2\Sigma_{\text{nl}}^2/2} + P_{\text{lin,nw}}(k) \quad (23)$$

<sup>11</sup> <https://ccpforge.cse.rl.ac.uk/gf/project/multinest/>

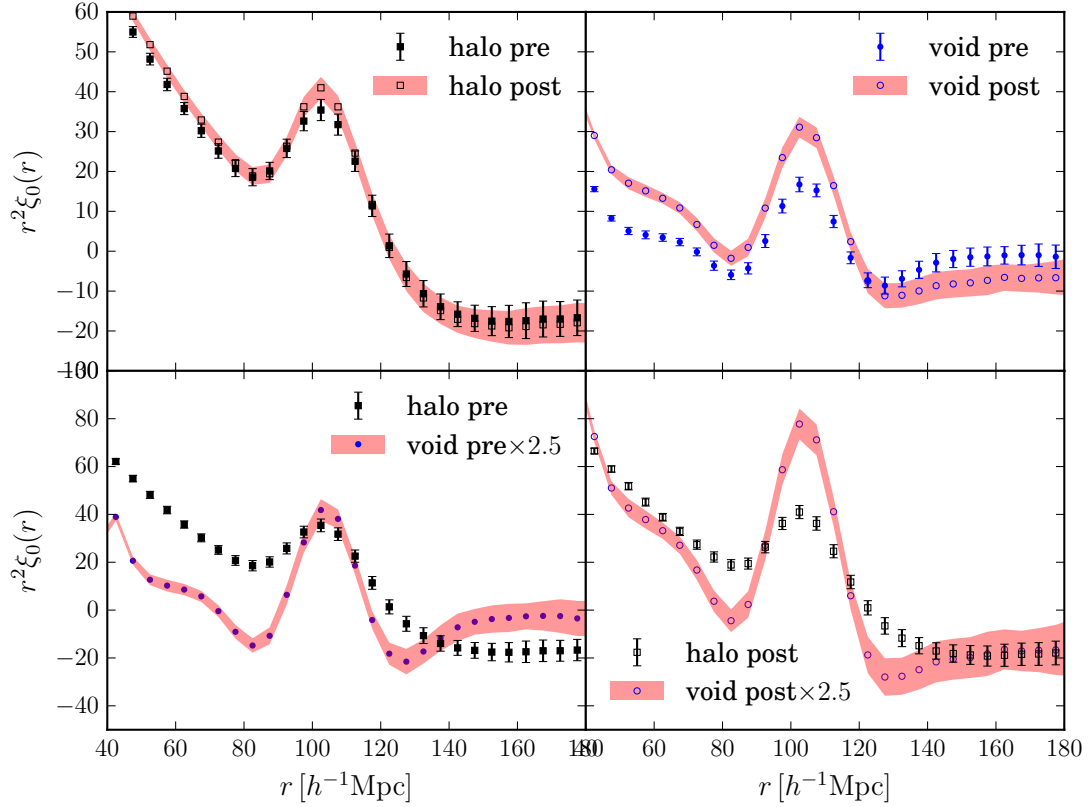


**Figure 2.** The comparisons of 2PCFs of haloes and voids from PATCHY cubic mocks. “pre” in the legends indicates results from the samples without BAO reconstruction, while “post” denotes results with BAO reconstruction. The error bars and shadowed bands show errors obtained from 100 realisations. For the comparisons between haloes and voids, we multiply the 2PCF of voids by a factor of 2.5 to obtain similar amplitudes on BAO scale.

**Table 4.** Fitted parameters for the mean 2PCF of 100 PATCHY cubic mocks with the improved BAO model expressed by Eq. 23.

Parameter	pre-recon		post-recon	
	Halo	Void	Halo	Void
$\bar{\alpha} - 1$	0.00394	-0.00159	0.00060	-0.00110
$\sigma_\alpha$	0.00389	0.00538	0.00276	0.00469
$\Sigma'_{nl}$	6.62	9.28	4.54	9.67
$c$	0.180	20126	0.00243	973.9
$B$	1.55	0.104	1.56	0.589
$\chi^2_{\min}$	0.198	1.09	0.173	0.703

#### 4.5 Fitting results with the modified de-wiggled model

We redo the analyses in §4.3, but replacing the BAO model with the modified one expressed in Eq. 23. The best-fit model curves for haloes and voids are shown in Figure 8 and Figure 9 respectively. The model curves for voids are much closer to the data compared to Figure 4.

We further list the fitted parameters in Table 4. For haloes, the fitted parameter  $c$  is too small to change the results of other parameters, i.e., the new model degenerates to the de-wiggled model. But with a large  $c$  for voids, the best-fit  $\chi^2$  is indeed greatly reduced. It shows that the improved BAO model works well for both haloes and voids.

Moreover, since the fiducial cosmology for the fittings is the “true” cosmology for generating the mocks, in principle

$\alpha$  should be exactly 1. However, Table 4 also shows opposite BAO shifts for haloes and voids. Note that the covariance matrix we use here indicates the error of a single realisation, but the fitted data is the mean 2PCF of 100 mocks. Therefore, considering only sample variance, the fitted error of the mean 2PCF should be  $\sim 10\%$  of that of a single realisation. In this case, the BAO shifts are statistically significant. Indeed, the opposite direction of BAO shifts for haloes and voids are consistent with theoretical predictions (Neyrinck et al. 2016). This further confirms that the BAO signal of our void sample is from under-dense regions.

We now examine the BAO fitting results for post-reconstruction mocks with the modified BAO model. The best-fit curves are shown in Figure 10, and the fitting results are listed in Table 4. Basically we obtain a  $\sim 30\%$  improvement on the error of the baryon acoustic scale constraint for haloes after BAO reconstruction. However, we do not observe any improvements for voids. It shows that BAO reconstruction does not contribute to a tighter BAO peak position constraint for voids. This may be due to the fact that we are using the optimal radius cut measured by Liang et al. (2016) using pre-reconstruction catalogues. It is likely that the optimal radius cut for the post-reconstruction catalogues is different. We shall study this effect in the future. Nevertheless, the BAO shifts of haloes and voids are both greatly reduced. This implies that a joint baryon acoustic scale constraint of haloes (or galaxies) and voids is likely to be unbiased.

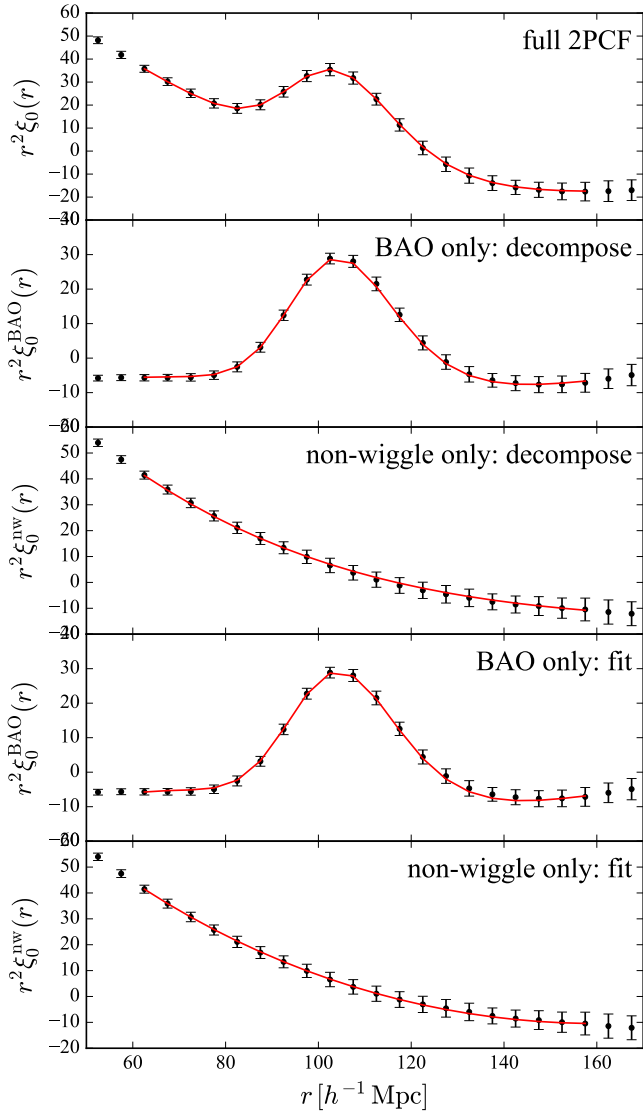


**Figure 3.** The mean and error of the 2PCFs from 100 PATCHY mock *halo* catalogues (black dots) as well as the best-fit model curves (red lines). The red lines in the second and third panels are directly decomposed from the best-fit curve of the full 2PCF (the first panel), while the ones for the last two panels are the best-fit results of the decomposed models.

## 5 MEASURING BAO BY COMBINING GALAXIES AND VOIDS

### 5.1 Correlation function estimator for the combined sample

Now we investigate the possibility of constructing a combined galaxy and void sample for baryon acoustic scale constraint. It has been shown that a population of the voids have negative bias, yielding a negative BAO peak in the cross correlation function of galaxies and voids (Liang et al. 2016). Therefore, if we simply compute the auto-correlation function of the joint data set of the galaxy and void tracers, the BAO signal will be smeared out. However, we can use a weighting scheme to assign different weights/signs to galaxies and voids.

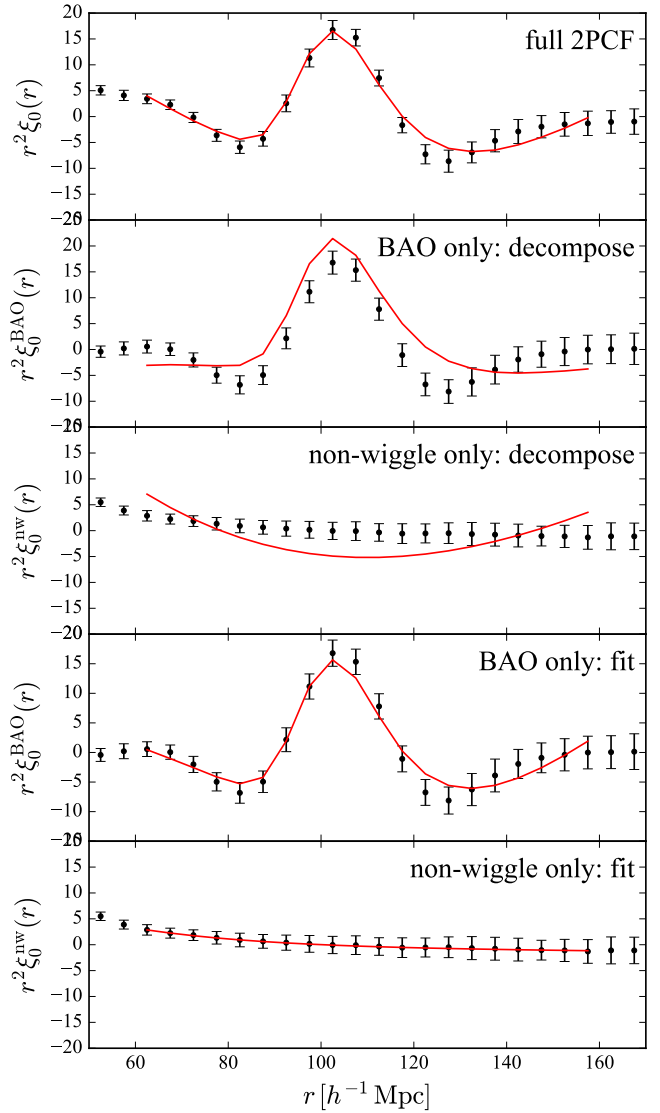


**Figure 4.** The mean and error of the 2PCFs from 100 PATCHY mock *void* catalogues (black dots) as well as the best-fit model curves (red lines). The red lines in the second and third panels are directly decomposed from the best-fit curve of the full 2PCF (the first panel), while the ones for the last two panels are the best-fit results of the decomposed models.

In this paper, we consider the simplest weighting scheme, i.e. assigning a constant weight  $w$  to the void tracers selected, while leaving galaxies without extra weights. Denoting the counting pairs for galaxies (voids) with subscript  $g$  ( $v$ ), and the number of galaxies and voids as  $n_g$  and  $n_v$  respectively. Then with the weight  $w$  for all the voids, the combined pair counts are

$$DD = \frac{D_g D_g \cdot n_g^2 + D_g D_v \cdot n_g n_v w + D_v D_v \cdot n_v^2 w^2}{(n_g + n_v w)^2}, \quad (24a)$$

$$DR = [D_g R_g \cdot n_g^2 + D_v R_v \cdot n_v^2 w^2 + (D_g R_v + D_v R_g) \cdot n_g n_v w / 2] / (n_g + n_v w)^2 \quad (24b)$$

$$RR = \frac{R_g R_g \cdot n_g^2 + R_v R_v \cdot n_v^2 w^2 + R_g R_v \cdot n_g n_v w}{(n_g + n_v w)^2}. \quad (24c)$$



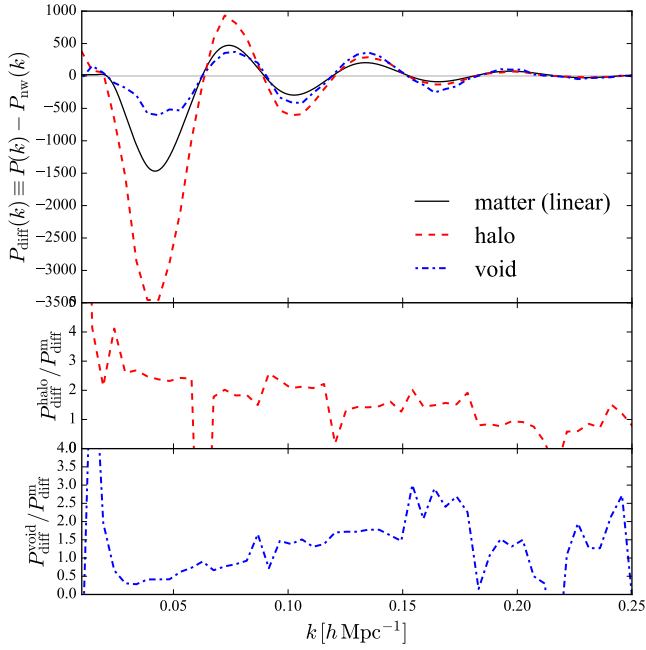


**Figure 5.** The wiggled components of the power spectra (computed by the difference of the normal power spectra and the non-wiggle ones) for dark matter in the linear regime, haloes, and voids (upper panel), together with the ratio of halo and void BAO to that of dark matter (middle and bottom panels). The increasing ratio in the bottom panel indicated that the wiggles of void clustering cannot be modelled by a damping of the linear wiggles.

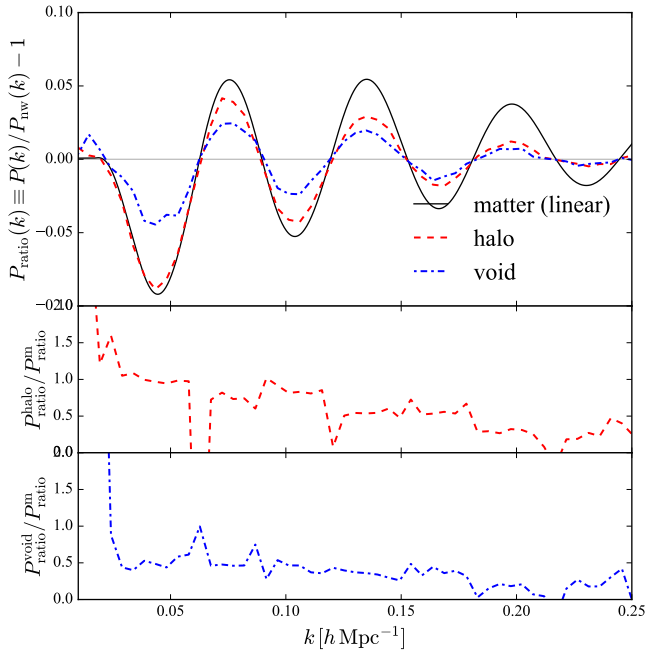


**Figure 6.** Same as Figure 5, but the wiggled components are computed by the ratio of the normal power spectra to the non-wiggle ones. It is possible to model the wiggles of voids using a damping of the linear wiggles in this case.

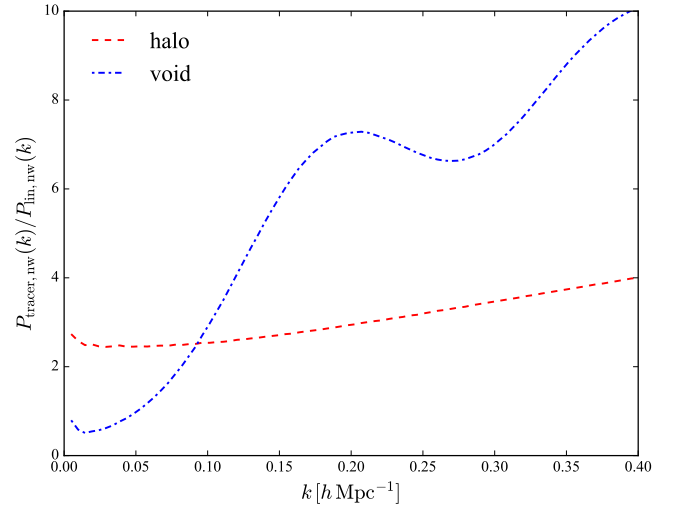


**Figure 7.** The ratio of the non-wiggle power spectra of haloes and voids from PATCHY mocks to that of linear dark matter. The curve of haloes can be approximated by a constant, which is not the case for the curve of voids.

Therefore, the combined correlation function is

$$\xi_{\text{comb}} = \frac{DD - 2DR + RR}{RR} = \frac{n_g^2 \xi_{\text{gg}} \cdot R_g R_g + n_v^2 w^2 \xi_{\text{vv}} \cdot R_v R_v + n_g n_v w \xi_{\text{gv}} \cdot R_g R_v}{n_g^2 \cdot R_g R_g + n_v^2 w^2 \cdot R_v R_v + n_g n_v w \cdot R_g R_v}, \quad (25)$$

where

$$\xi_{\text{gg}} = \frac{D_g D_g - 2D_g R_g + R_g R_g}{R_g R_g}, \quad (26a)$$

$$\xi_{\text{vv}} = \frac{D_v D_v - 2D_v R_v + R_v R_v}{R_v R_v}, \quad (26b)$$

$$\xi_{\text{gv}} = \frac{D_g D_v - D_g R_v - D_v R_g + R_g R_v}{R_g R_v}. \quad (26c)$$

Since the BAO peak position constraint from void alone is weaker than that of galaxy alone, the absolute value of the optimal weight for voids should be less than 1. We then vary  $w$  in the range  $w \in [-1, 1]$  and explore the optimal value by minimising the standard error of parameter  $\alpha$  ( $\sigma_\alpha$ ) when fitting to the combined sample.

## 5.2 Optimal combination of galaxies and voids

We rely on the post-reconstruction MD-PATCHY DR12 light-cone mocks for the optimal void weight searching. The 2PCFs of galaxies and voids in the high- $z$  bin are shown in Figure 11. As the case for haloes, we fit the BAO model to the mean of the 2PCFs of 1000 realisations. The fitting range we use in this section is  $s \in [50, 160] h^{-1} \text{Mpc}$ .

The fitted  $\alpha$  and  $\sigma_\alpha$  as a function of  $w$  for the high- $z$  and low- $z$  bins are shown in Figure 12 and Figure 13 respectively. One can see that for both redshift bins, in the weight range  $-0.1 < w < 0$ , the combined sample reduces the error on  $\alpha$ , without biasing it. In particular, the optimal weight  $w$  for both cases are  $-0.07$ . We show the best-fit curves of the galaxy sample, the void sample, and the combined sample

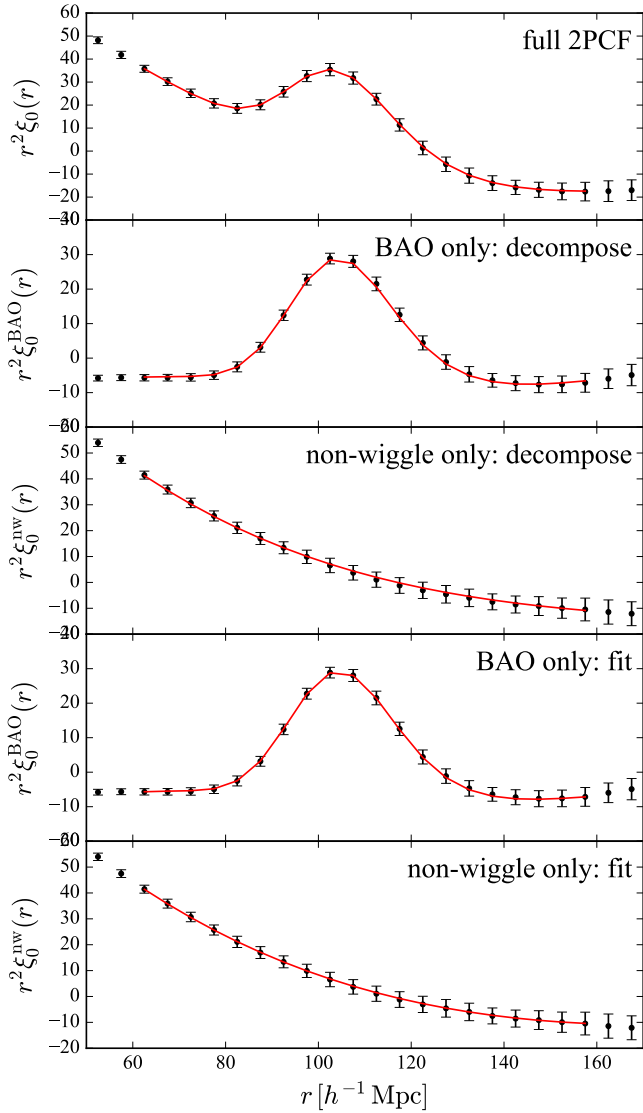


**Figure 8.** The mean and error of the 2PCFs from 100 Patchy mock *halo* catalogues (black dots) as well as the best-fit model curves (red lines) obtained from the improved BAO model (Eq. 23). See Figure 3 for a detailed description of the panels.

**Table 5.** The fitting results on  $\alpha$  for the mean 2PCF of 1000 MD-PATCHY light-cone mocks, of the galaxy sample, the void sample, and the combined sample with the void weight  $w = -0.07$ .

	$0.2 < z < 0.5$	$0.5 < z < 0.75$
galaxy	$0.9981 \pm 0.0133$	$0.9996 \pm 0.0124$
void	$0.9963 \pm 0.0202$	$1.0178 \pm 0.0575$
combined	$0.9982 \pm 0.0114$	$0.9998 \pm 0.0110$

with  $w = -0.07$  in Figure 14 and Figure 15 for the two redshift bins. The fitting results are listed in Table 5.

The numbers for the galaxy samples in Table 5 are consistent with the results in Vargas-Magaña et al. (2016), with the same sets of mocks. Using the combined sample, we obtain 11.1% and 13.7% improvements than the galaxy sample on the precision of baryon acoustic scale constraints for the high- $z$  bin and low- $z$  bin respectively. These amounts of

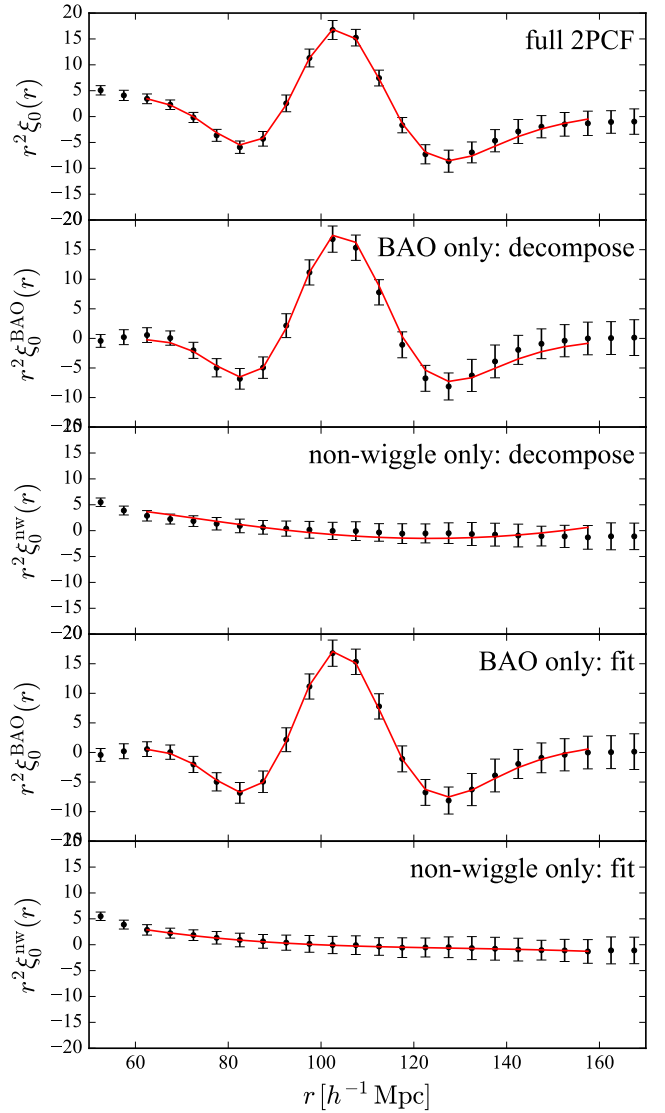


**Figure 9.** The mean and error of the 2PCFs from 100 Patchy mock *void* catalogues (black dots) as well as the best-fit model curves (red lines) obtained from the improved BAO model (Eq. 23). See Figure 4 for a detailed description of the panels.

improvement correspond to effectively enlarging the sample by more than 20%.

It implies that voids help on extracting more cosmological information from troughs of the underlying density field, which is complementary to galaxies. To examine the robustness of the conclusion in terms of the number of mocks, we further divide our mock sample into two independent sub-samples with 500 mocks, and both of the sub-samples yield the same result as the full sample.

### 5.3 Measurements from observed galaxies and voids

We now take the optimal void weight obtained from MD-PATCHY mocks ( $w = -0.07$ ), and apply it to the corresponding BOSS DR12 data. The best-fit curves are shown

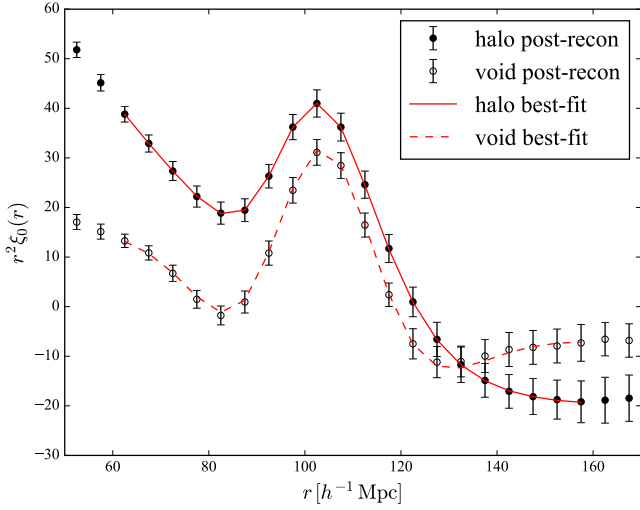


**Figure 10.** The mean and error of the 2PCFs from 100 PATCHY post-reconstruction mock halo/void catalogues (black solid/open dots) as well as the best-fit model curves (red solid/dash lines) obtained from the modified BAO model.

**Table 6.** The fitting results on  $\alpha$  for the BOSS DR 12 data of the galaxy sample, the void sample, and the combined sample with the void weight  $w = -0.07$ .

	$0.2 < z < 0.5$	$0.5 < z < 0.75$
galaxy	$0.9967 \pm 0.0092$	$0.9801 \pm 0.0094$
void	$0.9842 \pm 0.0173$	$0.9979 \pm 0.0315$
combined	$0.9934 \pm 0.0081$	$0.9814 \pm 0.0102$

in Figure 16 and Figure 17 for the high- $z$  and low- $z$  bins respectively. The BAO measurements are listed in Table 6.

Results for the galaxy samples in Table 6 are again consistent with those in Vargas-Magaña et al. (2016). Compared to the galaxy sample, the combined sample shows an 11.6% percent improvement on the error of baryon acoustic scale constraint, which is roughly the expectation value from the results on MD-PATCHY mocks. However, the high- $z$  bin does not show any improvements with voids. Indeed the results for the combined sample is even worse. The next section explains that this result is compatible with statistical fluctuations with present statistics.

#### 5.4 Statistical fluctuations on the improvements with voids

In this section, we measure the BAO constraints from individual mocks to study the distribution of the improvement on baryon acoustic scale constraint. Denoting  $\sigma_{\alpha, \text{galaxy}}$  as the fitted error on  $\alpha$  for the galaxy sample, and  $\sigma_{\alpha, \text{combined}}$  as the result from the combined sample with the void weight of  $w = -0.07$ , we define the relative improvement on the constraint as  $(\sigma_{\alpha, \text{combined}} - \sigma_{\alpha, \text{galaxy}}) / \sigma_{\alpha, \text{galaxy}}$ . In this case a negative value indicates that we have improvements.

We plot the distribution of the relative improvement on the BAO scale constraint from the 1000 MD-PATCHY mocks in Figure 18 and Figure 19 for the high- $z$  and low- $z$  redshift bins respectively. One can see that for both cases, the

relative improvement value of the BOSS DR12 data is not located far away from the peak. Therefore, we conclude that the failure of improvement with voids for the high- $z$  bin is consistent with statistical fluctuations (cosmic variance). Indeed, for the high- $z$  bin, 71.5% of the mocks show improvements on BAO scale constraint with voids. The percentage is 75.9% for the low- $z$  bin.

Then, we explore the performance of our method for future surveys with larger volumes (smaller statistical fluctuations) by taking the mean 2PCF of every 10 mocks, to have a larger effective volume for each 2PCF. With the 100 realisations of 2PCFs, we apply the modified de-wiggled model and obtain the relative improvement on the BAO scale constraint with voids. The distribution for the high- $z$  bin is shown in Figure 20, which shows a much smaller FWHM than that in Figure 18. Furthermore, we have a worse constraint on  $\alpha$  for only one realisation (1%) in this case. This indicates that our method is more promising for a larger sample size.

## 6 CONCLUSIONS

In this paper, we focus on the BAO peak position constraints from void clustering statistics, and the consequences when combined with halo/galaxy data on the determination of cosmological parameters. We first perform a theoretical and ideal study using 100 realisations of cubic PATCHY mocks. To reduce the statistical fluctuations induced by a single realisation, we apply the analyses to the mean of 2PCFs from the 100 mocks, with the error being at one realisation level. From this test, we find the BAO peak position constraint from voids weaker, but comparable to that from haloes without performing BAO reconstruction. We further evidence a BAO position shift of voids towards the opposite direction compared to that of haloes. This in turn confirms that the BAO signal from voids is indeed from the density troughs of the cosmic field.

We then apply the BAO reconstruction method (Eisenstein et al. 2007; Padmanabhan et al. 2012) to the haloes from PATCHY cubic mocks, with a smoothing length of  $5 h^{-1} \text{Mpc}$ . In this way we find the BAO peak position constraint from haloes improved by  $\sim 30\%$ . Besides, the BAO shift of haloes is corrected. Later, we apply our void finder to the reconstructed haloes, and construct in this way a post-reconstruction void sample. However, we do not find improvement of BAO peak position constraint with voids. Nevertheless, the BAO shift of voids is also greatly reduced. The BAO position of haloes and voids are now more consistent than the pre-reconstruction results.

This consistency allows us to perform a joint constraint using both haloes and voids. To this end, we use 1000 realisations of post-reconstruction MultiDark PATCHY DR12 mocks, which are calibrated to mimic the BOSS DR12 observational data. Since the BAO peak position of haloes in the cubic mocks is more robust, we treat galaxies as our basis, and study the contribution of voids. Therefore, we apply a single weight  $w$  to the whole void sample, and vary it from  $-1$  to  $1$  to combine with galaxies, and study the BAO position constraint of the joint sample. In this way, we find an optimal void weight of  $w = -0.07$  for both low- $z$  and high- $z$  redshift bins. With the weight near this value, we minimise the fitted error of BAO peak position, with-

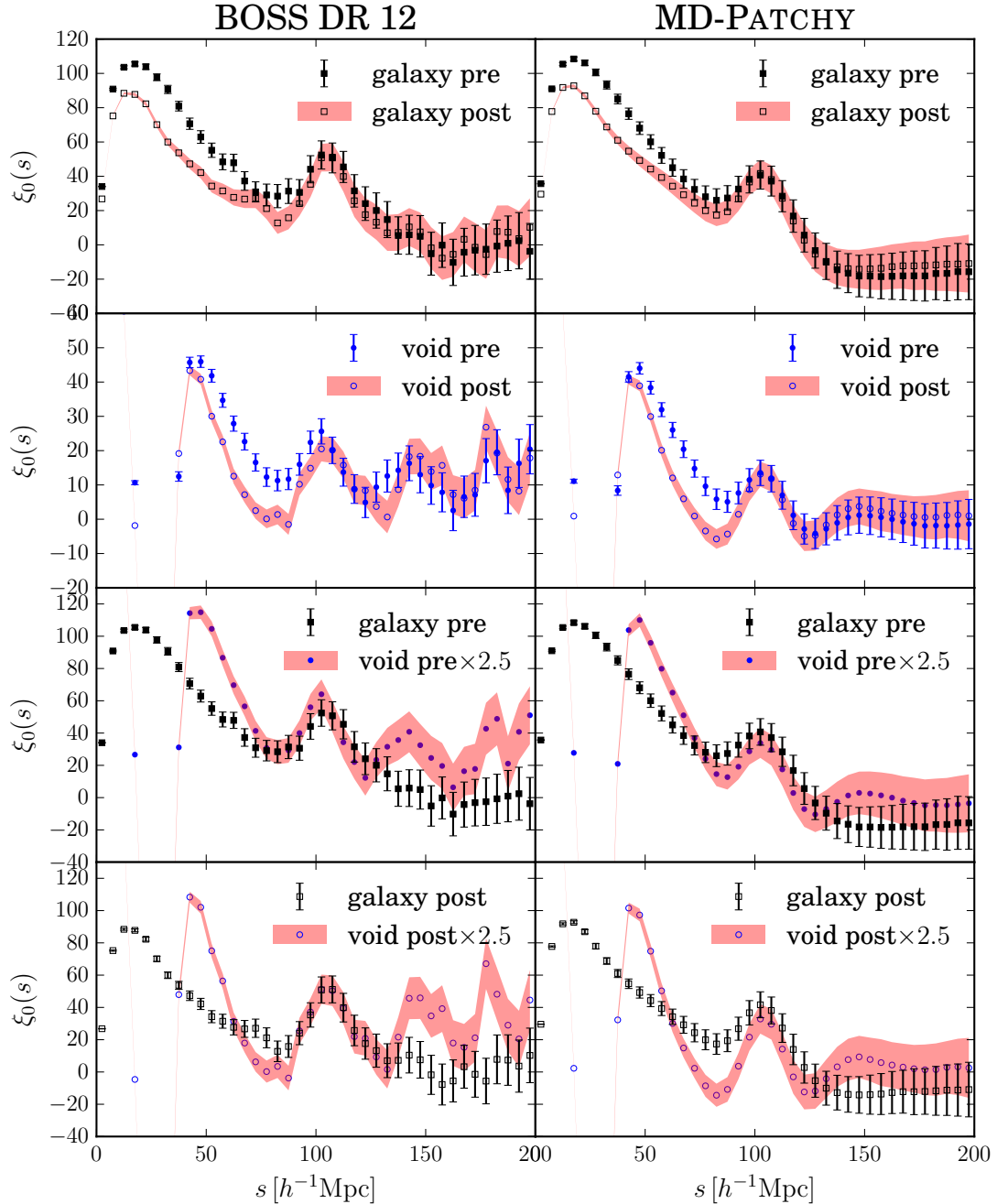


**Figure 11.** Comparisons of the 2-point correlation functions of pre- and post-reconstruction galaxies and voids in the redshift bin  $0.5 < z < 0.75$ . “pre” and “post” in the legends are referred to the results from pre-reconstruction and post-reconstruction samples respectively. The error bars and shadowed bands show the error obtained from 1000 realisations of mocks. For the comparisons between galaxies and voids, we multiply the 2PCF of voids by a factor of 2.5 to obtain similar amplitudes on BAO scale.

out biasing it. Moreover, with this optimal weight, we find 13.7% and 11.1% improvement on the error of BAO peak position than that from the galaxy sample alone, for the low- $z$  and high- $z$  sample respectively. We further divide the 1000 mocks to 2 independent sets of 500 realisations, and observe the same level of improvements. This ensures that the improvements are indeed from our void sample, rather than statistical fluctuations. These levels of improvements are equivalent to enlarging over 20% of the sample size, while we do not require any extra inputs other than those for galaxy BAO analyses.

We finally apply the void weight to the BOSS DR12 data, and find an 11.6% improvement on the BAO position constraint for the low- $z$  data. However, we do not observe any improvement for the high- $z$  data, and the constraint from the joint sample is even worse. By studying the performance of our method for the 1000 individual mocks, we find the influence of cosmic variance not negligible. And the failure of improvement for the high- $z$  sample is consistent with statistical fluctuations from a single realisation. Furthermore, the improvement on the BAO scale constraint is more robust for a larger sample size.

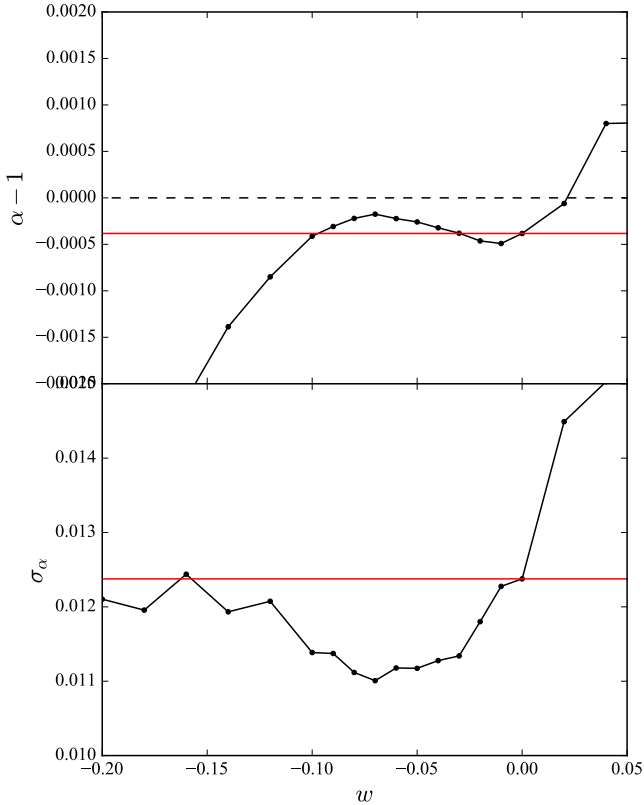


**Figure 12.** The fitted  $\alpha$  and the error on  $\alpha$  as a function of the weight of voids for the mean of 1000 MD-PATCHY mocks in the redshift bin  $0.5 < z < 0.75$ . The red solid lines show the results from galaxies alone.

We leave the application on cosmological parameter constraints using our method to a future paper. More detailed weighting schemes for combining galaxies and voids will be investigated in forthcoming work.

## ACKNOWLEDGMENTS

We thank Prof. Houjun Mo for useful discussions. CZ, YL, and CT are supported by Tsinghua University with a 985 grant, 973 programme 2013CB834906, NSFC grant No. 11033003 and 11173017, and sino french CNRS-CAS international laboratories LIA Origins and FCPPL. CZ also acknowledges supports from NSFC grant No. 11673025 and a Royal Society Newton Advanced Fellowship. FSK thanks support from the grants RYC2015–18693 and AYA2017-89891-P. GY acknowledges financial support from the *Ministerio de Economía y Competitividad* and the *Fondo Europeo de Desarrollo Regional* (MINECO/FEDER, UE) in Spain through grant AYA2015-63810-P. MVM is partially supported by Programa de Apoyo a Proyectos de Investigación e Innovación Tecnológica (PAPITT) No. IA102516, Proyecto Conacyt Fronteras No. 281 and from Proyecto LANCAD-UNAM-DGTIC-319.

The computations have been performed on the MARENOSTRUM supercomputer at the Barcelona Supercomputing Centre, thanks to the computing time awarded by Red Española de Supercomputación. We also acknowl-

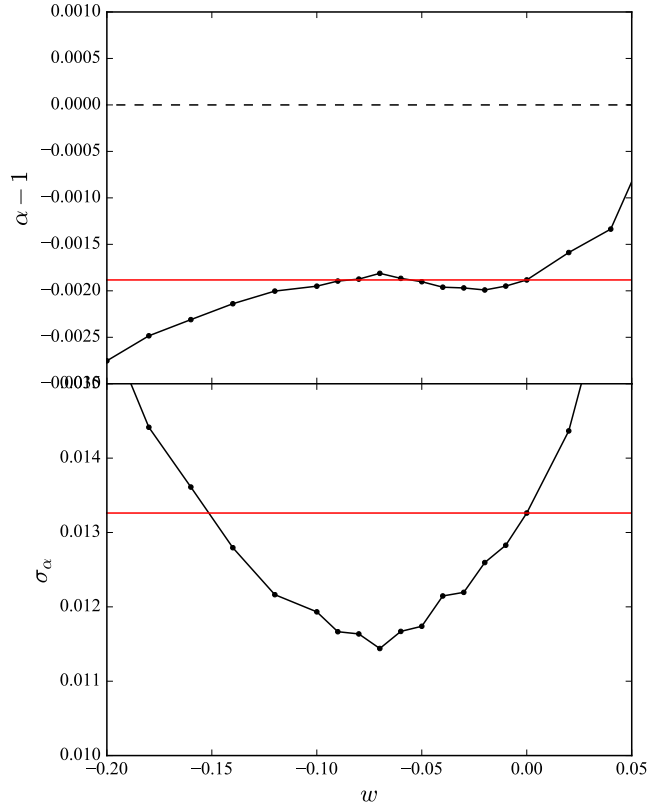


**Figure 13.** The fitted  $\alpha$  and the error on  $\alpha$  as a function of the weight of voids for the mean of 1000 MD-PATCHY mocks in the redshift bin  $0.2 < z < 0.5$ . The red solid lines show the results from galaxies alone.

edge the HPC facilities BEILUO at Tsinghua University and EREBOS/THEIA/GERAS at Leibniz-Institut für Astrophysik Potsdam for some of the computations.

Funding for SDSS-III has been provided by the Alfred P. Sloan Foundation, the Participating Institutions, the National Science Foundation, and the U.S. Department of Energy Office of Science. The SDSS-III web site is <http://www.sdss3.org/>.

SDSS-III is managed by the Astrophysical Research Consortium for the Participating Institutions of the SDSS-III Collaboration including the University of Arizona, the Brazilian Participation Group, Brookhaven National Laboratory, Carnegie Mellon University, University of Florida, the French Participation Group, the German Participation Group, Harvard University, the Instituto de Astrofísica de Canarias, the Michigan State/Notre Dame/JINA Participation Group, Johns Hopkins University, Lawrence Berkeley National Laboratory, Max Planck Institute for Astrophysics, Max Planck Institute for Extraterrestrial Physics, New Mexico State University, New York University, Ohio State University, Pennsylvania State University, University of Portsmouth, Princeton University, the Spanish Participation Group, University of Tokyo, University of Utah, Vanderbilt University, University of Virginia, University of Washington, and Yale University.

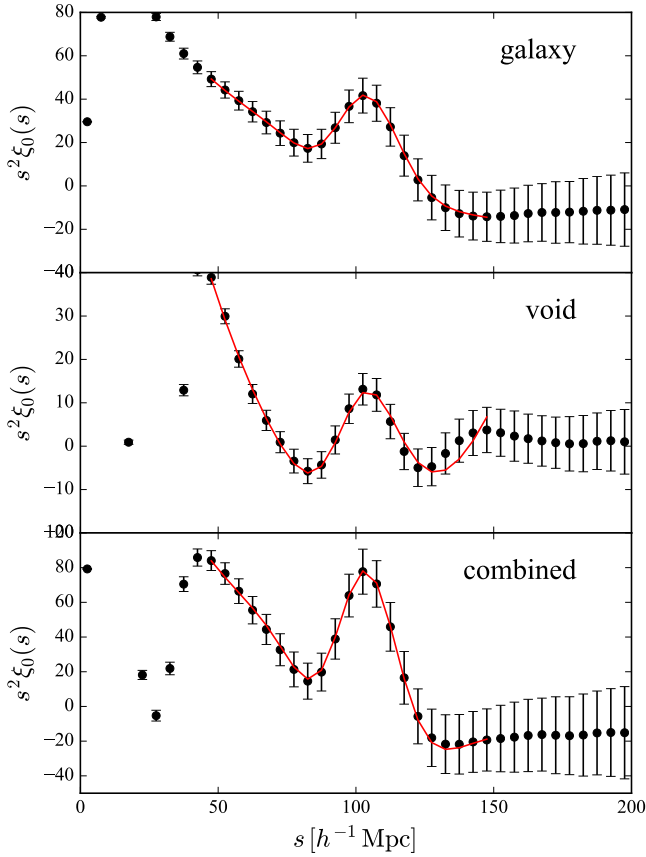


**Figure 14.** The best-fit curves for the mean of 1000 MD-PATCHY mocks of the galaxy sample, the void sample, and the combined sample with  $w = -0.07$  for the redshift bin  $0.5 < z < 0.75$ .

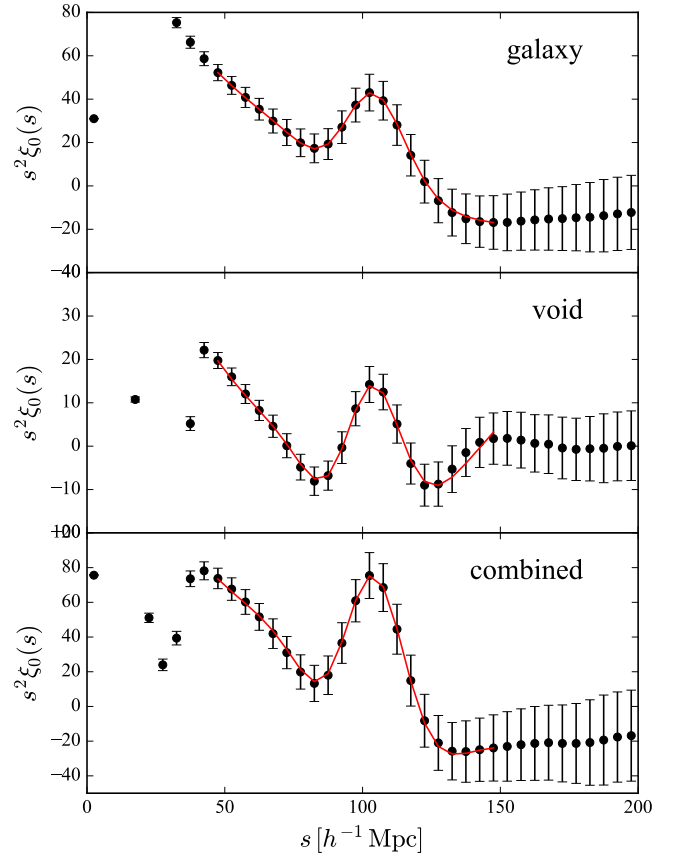


**Figure 15.** The best-fit curves for the mean of 1000 MD-PATCHY mocks of the galaxy sample, the void sample, and the combined sample with  $w = -0.07$  for the redshift bin  $0.2 < z < 0.5$ .

## REFERENCES

- Abramo L. R., Leonard K. E., 2013, *MNRAS*, **432**, 318  
Achitouv I., Blake C., 2015, *Phys. Rev. D*, **92**, 083523  
Alam S., et al., 2017, *MNRAS*, **470**, 2617  
Anderson L., et al., 2012, *MNRAS*, **427**, 3435  
Anderson L., et al., 2014, *MNRAS*, **441**, 24  
Ata M., et al., 2017, preprint ([arXiv:1705.06373](https://arxiv.org/abs/1705.06373))  
Benitez N., et al., 2014, preprint ([arXiv:1403.5237](https://arxiv.org/abs/1403.5237))  
Bernstein G. M., Cai Y.-C., 2011, *MNRAS*, **416**, 3009  
Blake C., Glazebrook K., 2003, *ApJ*, **594**, 665  
Bolton A. S., et al., 2012, *AJ*, **144**, 144  
Burden A., Percival W. J., Manera M., Cuesta A. J., Vargas Magana M., Ho S., 2014, *MNRAS*, **445**, 3152  
Busca N. G., et al., 2013, *A&A*, **552**, A96  
Chang T.-C., Pen U.-L., Peterson J. B., McDonald P., 2008, *Physical Review Letters*, **100**, 091303  
Chuang C.-H., et al., 2015, *MNRAS*, **452**, 686  
Chuang C.-H., Kitaura F.-S., Liang Y., Font-Ribera A., Zhao C., McDonald P., Tao C., 2017, *Phys. Rev. D*, **95**, 063528  
Colberg J. M., et al., 2008, *MNRAS*, **387**, 933  
Cole S., et al., 2005, *MNRAS*, **362**, 505  
Croft R. A. C., Gaztanaga E., 1997, *MNRAS*, **285**, 793  
Dark Energy Survey Collaboration et al., 2016, *MNRAS*, **460**, 1270  
Dawson K. S., et al., 2013, *AJ*, **145**, 10  
Dawson K. S., et al., 2016, *AJ*, **151**, 44  
Delaunay B., 1934, *Izv. Akad. Nauk SSSR, Otdelenie Matematicheskii i Estestvennyka Nauk*, **7**, 1  
Eisenstein D. J., Hu W., 1998, *ApJ*, **496**, 605

- Eisenstein D. J., et al., 2005, *ApJ*, **633**, 560  
Eisenstein D. J., Seo H.-J., Sirko E., Spergel D. N., 2007, *ApJ*, **664**, 675  
Eisenstein D. J., et al., 2011, *AJ*, **142**, 72  
El-Ad H., Piran T., 1997, *ApJ*, **491**, 421  
Feldman H. A., Kaiser N., Peacock J. A., 1994, *ApJ*, **426**, 23  
Feroz F., Hobson M. P., 2008, *MNRAS*, **384**, 449  
Feroz F., Hobson M. P., Bridges M., 2009, *MNRAS*, **398**, 1601  
Feroz F., Hobson M. P., Cameron E., Pettitt A. N., 2013, preprint ([arXiv:1306.2144](https://arxiv.org/abs/1306.2144))  
Ferraro S., Sherwin B. D., Spergel D. N., 2015, *Phys. Rev. D*, **91**, 083533  
Gil-Marín H., Wagner C., Verde L., Jimenez R., Heavens A. F., 2010, *MNRAS*, **407**, 772  
Hamaus N., Seljak U., Desjacques V., 2011, *Phys. Rev. D*, **84**, 083509  
Hamaus N., Seljak U., Desjacques V., 2012, *Phys. Rev. D*, **86**, 103513  
Hamaus N., Wandelt B. D., Sutter P. M., Lavaux G., Warren M. S., 2014, *Physical Review Letters*, **112**, 041304  
Hartlap J., Simon P., Schneider P., 2007, *A&A*, **464**, 399  
Jasche J., Wandelt B. D., 2013, *MNRAS*, **432**, 894  
Kaiser N., 1984, *ApJ*, **284**, L9  
Kazin E. A., et al., 2014, *MNRAS*, **441**, 3524  
Kitaura F.-S., 2013, *MNRAS*, **429**, L84  
Kitaura F. S., Enßlin T. A., 2008, *MNRAS*, **389**, 497  
Kitaura F.-S., Heß S., 2013, *MNRAS*, **435**, L78  
Kitaura F.-S., Yepes G., Prada F., 2014, *MNRAS*, **439**, L21  
Kitaura F.-S., Gil-Marín H., Scóccola C. G., Chuang C.-H., Müller

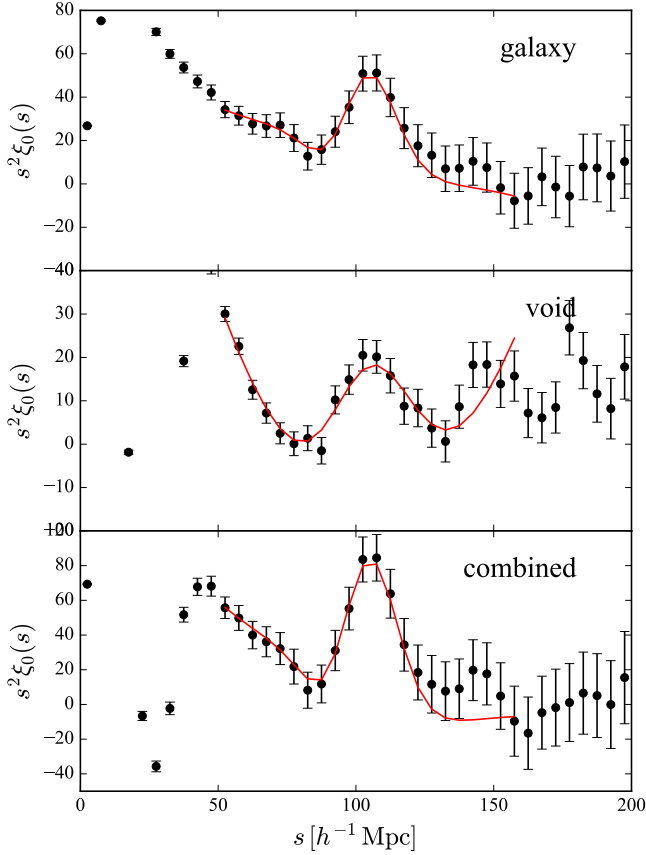


**Figure 16.** The best-fit curves for the BOSS DR12 data of the galaxy sample, the void sample, and the combined sample with  $w = -0.07$  in the redshift bin  $0.5 < z < 0.75$ .

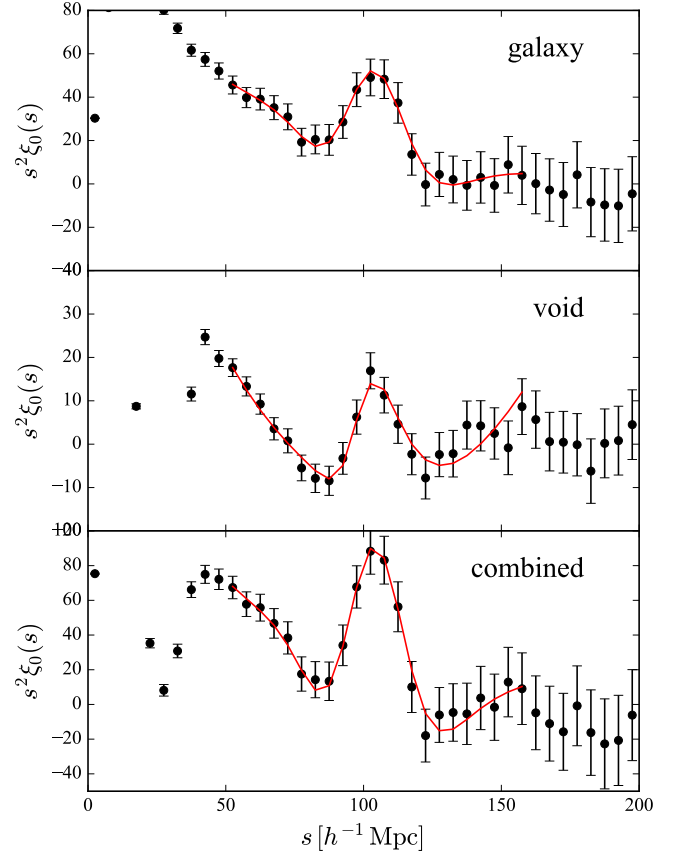


**Figure 17.** The best-fit curves for the BOSS DR12 data of the galaxy sample, the void sample, and the combined sample with  $w = -0.07$  in the redshift bin  $0.2 < z < 0.5$ .

- V., Yepes G., Prada F., 2015, *MNRAS*, **450**, 1836  
 Kitaura F.-S., et al., 2016a, *Physical Review Letters*, **116**, 171301  
 Kitaura F.-S., et al., 2016b, *MNRAS*, **456**, 4156  
 Kitaura F.-S., Ata M., Angulo R. E., Chuang C.-H., Rodríguez-Torres S., Monteagudo C. H., Prada F., Yepes G., 2016c, *MNRAS*, **457**, L113  
 Klypin A., Yepes G., Gottlober S., Prada F., Hess S., 2014, preprint ([arXiv:1411.4001](https://arxiv.org/abs/1411.4001))  
 LSST Dark Energy Science Collaboration 2012, preprint ([arXiv:1211.0310](https://arxiv.org/abs/1211.0310))  
 Landy S. D., Szalay A. S., 1993, *ApJ*, **412**, 64  
 Laureijs R., et al., 2011, preprint ([arXiv:1110.3193](https://arxiv.org/abs/1110.3193))  
 Levi M., et al., 2013, preprint ([arXiv:1308.0847](https://arxiv.org/abs/1308.0847))  
 Lewis A., Challinor A., Lasenby A., 2000, *Astrophys. J.*, **538**, 473  
 Liang Y., Zhao C., Chuang C.-H., Kitaura F.-S., Tao C., 2016, *MNRAS*, **459**, 4020  
 Mohayaee R., Sobolevskii A., 2008, *Physica D Nonlinear Phenomena*, **237**, 2145  
 Neyrinck M. C., Szapudi I., McCullagh N., Szalay A., Falck B., Wang J., 2016, preprint ([arXiv:1610.06215](https://arxiv.org/abs/1610.06215))  
 Noh Y., White M., Padmanabhan N., 2009, *Phys. Rev. D*, **80**, 123501  
 Nuza S. E., et al., 2013, *MNRAS*, **432**, 743  
 Padmanabhan N., White M., Cohn J. D., 2009, *Phys. Rev. D*, **79**, 063523  
 Padmanabhan N., Xu X., Eisenstein D. J., Scalzo R., Cuesta A. J., Mehta K. T., Kazin E., 2012, *MNRAS*, **427**, 2132  
 Percival W. J., et al., 2014, *MNRAS*, **439**, 2531  
 Press W. H., Teukolsky S. A., Vetterling W. T., Flannery B. P.,

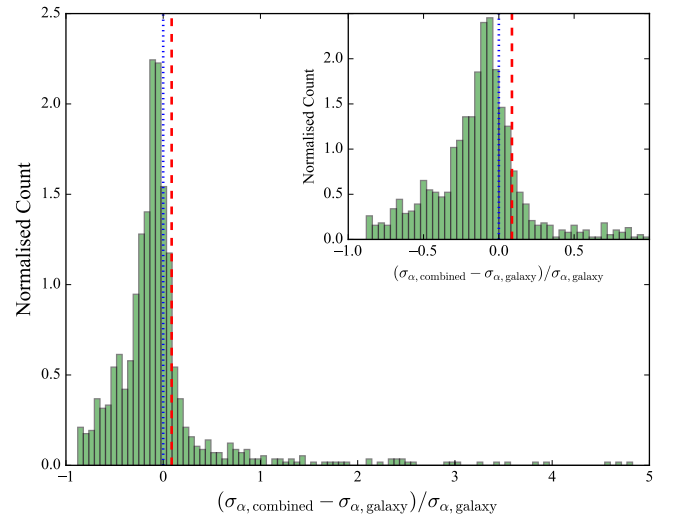


**Figure 18.** The distribution of baryon acoustic scale constraint improvement with voids in the redshift bin  $0.5 < z < 0.75$ . The blue dotted line indicates the limit of no improvement, and the red dash line shows the improvement for BOSS DR12 data.

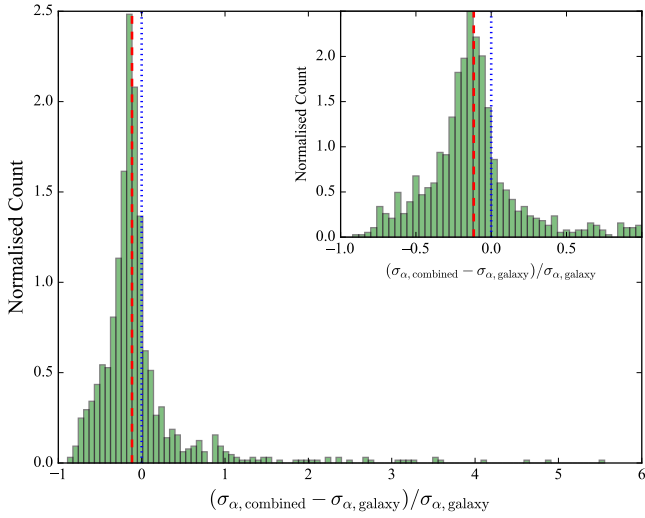


**Figure 19.** The distribution of baryon acoustic scale constraint improvement with voids in the redshift bin  $0.2 < z < 0.5$ . The blue dotted line indicates the limit of no improvement, and the red dash line shows the improvement for BOSS DR12 data.

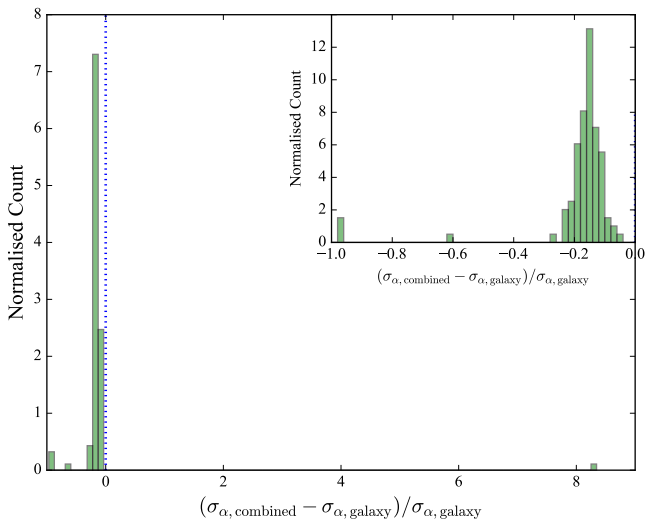


**Figure 20.** The distribution of baryon acoustic scale constraint improvement with voids in the redshift bin  $0.5 < z < 0.75$ , obtained from the mean of every 10 mocks. The blue dotted line indicates the limit of no improvement.

2007, Numerical Recipes 3rd Edition: The Art of Scientific Computing, 3 edn. Cambridge University Press, New York, NY, USA

- Reid B., et al., 2016, *MNRAS*, **455**, 1553  
 Rodríguez-Torres S. A., et al., 2016, *MNRAS*, **460**, 1173  
 Ross A. J., et al., 2012, *MNRAS*, **424**, 564  
 Ross A. J., et al., 2017, *MNRAS*, **464**, 1168  
 Schmittfull M., Feng Y., Beutler F., Sherwin B., Chu M. Y., 2015, *Phys. Rev. D*, **92**, 123522  
 Schmittfull M., Baldauf T., Zaldarriaga M., 2017, *Phys. Rev. D*, **96**, 023505  
 Seo H.-J., Eisenstein D. J., 2005, *ApJ*, **633**, 575  
 Sheth R. K., van de Weygaert R., 2004, *MNRAS*, **350**, 517  
 Spergel D., et al., 2013, preprint ([arXiv:1305.5422](https://arxiv.org/abs/1305.5422))

- Tassev S., Zaldarriaga M., 2012, *J. Cosmology Astropart. Phys.*, **10**, 006  
 Vargas-Magaña M., Ho S., Fromenteau S., Cuesta A. J., 2015, preprint ([arXiv:1509.06384](https://arxiv.org/abs/1509.06384))  
 Vargas-Magaña M., et al., 2016, preprint ([arXiv:1610.03506](https://arxiv.org/abs/1610.03506))  
 Wang H., Mo H. J., Yang X., van den Bosch F. C., 2013, *ApJ*, **772**, 63  
 Wang X., Yu H.-R., Zhu H.-M., Yu Y., Pan Q., Pen U.-L., 2017, *ApJ*, **841**, L29  
 Way M. J., Gazis P. R., Scargle J. D., 2015, *ApJ*, **799**, 95  
 Weinberg D. H., 1992, *MNRAS*, **254**, 315  
 Xu X., Padmanabhan N., Eisenstein D. J., Mehta K. T., Cuesta A. J., 2012, *MNRAS*, **427**, 2146  
 Zaroubi S., Hoffman Y., Fisher K. B., Lahav O., 1995, *ApJ*, **449**, 446  
 Zel'dovich Y. B., 1970, *A&A*, **5**, 84  
 Zhao C., Kitaura F.-S., Chuang C.-H., Prada F., Yepes G., Tao C., 2015, *MNRAS*, **451**, 4266  
 Zhao C., Tao C., Liang Y., Kitaura F.-S., Chuang C.-H., 2016, *MNRAS*, **459**, 2670  
 de Jong R. S., et al., 2012, in Ground-based and Airborne Instrumentation for Astronomy IV. p. 84460T ([arXiv:1206.6885](https://arxiv.org/abs/1206.6885)), doi:10.1117/12.926239  
 van de Weygaert R., Platen E., 2011, in International Journal of Modern Physics Conference Series. pp 41–66 ([arXiv:0912.2997](https://arxiv.org/abs/0912.2997)), doi:10.1142/S2010194511000092

## APPENDIX A: FITTING RANGE

To explore the impact of the fitting range on the baryon acoustic scale constraints, we vary the lower bound in the range  $s_{\min} \in [30, 80] h^{-1} \text{Mpc}$  and the upper bound in range  $s_{\max} \in [120, 190] h^{-1} \text{Mpc}$  with the bin size of  $5 h^{-1} \text{Mpc}$  for both cases. We then apply our BAO fitting procedure to the mean of 1000 MD-PATCHY light-cone mocks. The fitting results, including  $\alpha$ ,  $\sigma_\alpha$ , and the reduced  $\chi^2$  ( $\chi^2$  divided by the degree of freedom), of the galaxy sample, the void sample, and the combined sample with the void weight  $w = -0.07$  are shown in Figure A1 and Figure A2 for the high- $z$  and low- $z$  redshift bins respectively. Note that the covariance matrices we use are for single realisations, hence we should rescale the  $\chi^2$  by a factor of  $\sqrt{1000}$ .

It can be seen that the fitting results for voids are very sensitive to the fitting range. However, the results for the galaxy sample and the combined sample are both robust for  $s_{\min} \in [50, 65] h^{-1} \text{Mpc}$  and  $s_{\max} \in [160, 190] h^{-1} \text{Mpc}$ . We finally choose the fitting range  $s \in [50, 160] h^{-1} \text{Mpc}$  in this work. Indeed, we have also checked the optimal weight for several different fitting ranges, and find it not varying. This further confirms that our results are robust with respect to the fitting range.

This paper has been typeset from a  $\text{T}_\text{E}\text{X}/\text{L}^\text{A}\text{T}_\text{E}\text{X}$  file prepared by the author.



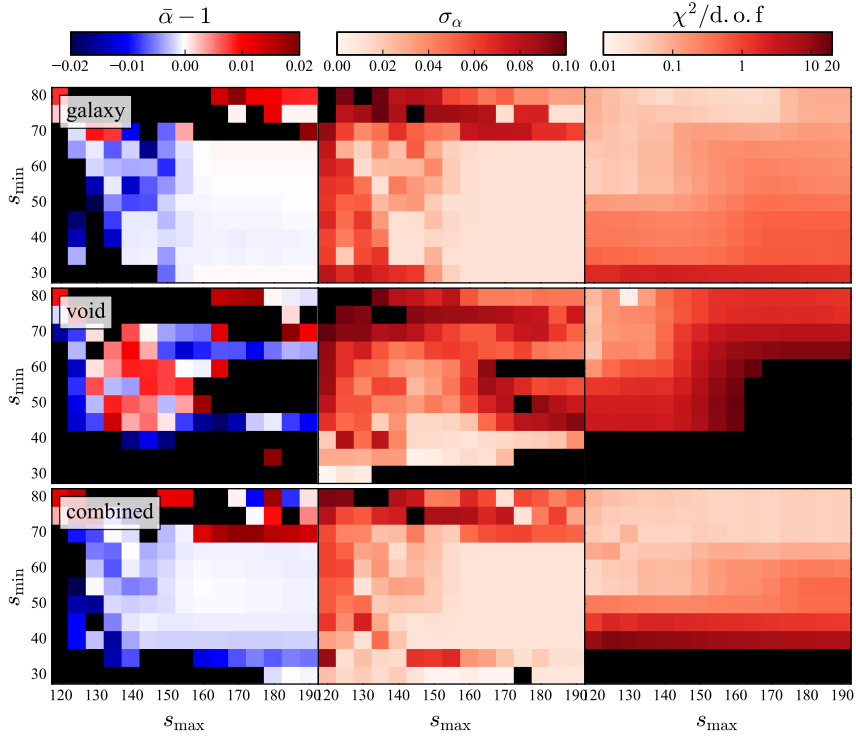


**Figure A1.** The BAO fitting results with different fitting ranges for the mean of 1000 MD-PATCHY light-cone mocks in the redshift bin  $0.5 < z < 0.75$ . We have taken into account the factor of  $\sqrt{1000}$  when computing the reduced  $\chi^2$ .

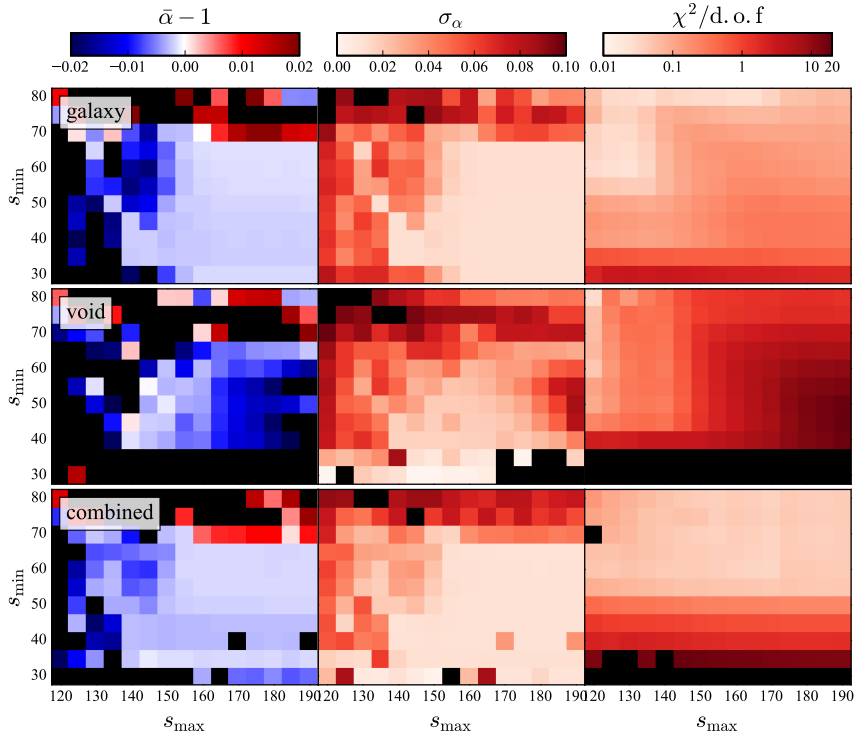


**Figure A2.** The BAO fitting results with different fitting ranges for the mean of 1000 MD-PATCHY light-cone mocks in redshift bin  $0.2 < z < 0.5$ . We have taken into account the factor of  $\sqrt{1000}$  when computing the reduced  $\chi^2$ .